

Deanship of Graduate studies

AL-Quds University

Modeling of electrical parameters in the vortex and  
superconducting states of  $\text{Bi}_2\text{Sr}_2\text{CaCu}_2\text{O}_x$  thick tapes

Inas Aref Naser

M. Sc. Thesis

Jerusalem-Palestine

2004

Modeling of electrical parameters in the vortex and  
superconducting states of  $\text{Bi}_2\text{Sr}_2\text{CaCu}_2\text{O}_x$  thick tapes

By

Inas Naser

(B. Sc. in Physics from AL-Quds University, Palestine)

A thesis Submitted in Partial Fulfillment of Requirements  
for the Degree of Master of Science, Department of  
Physics / College of Science and Technology

Al-Quds University

October, 2004

Program of Graduate Studies in Physics  
Deanship of Graduate Studies

## **Modeling of electrical parameters in the vortex and superconducting states of $\text{Bi}_2\text{Sr}_2\text{CaCu}_2\text{O}_x$ thick tapes**

By:

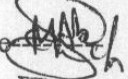
Student Name: Inas Naser

Registration No.: 20120280

Supervisor: Prof. Dr. Abdelkarim M. Saleh

Master thesis submitted and accepted, Date: 10/10/2004

The names and signatures of the examining committee members are as follows:

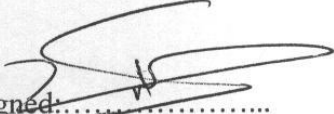
1- Prof. Dr. Abdelkarim M. Saleh	Head of committee	Signature- 
2- Dr. Mohammad M. Abu-Samreh	Internal Examiner	Signature- 
3- Dr. Jamal Sulaiman	External Examiner	Signature- 

Al-Quds University

2004-2005

## **DECLARATION**

I certify that this thesis, which is submitted for the degree of master, is the result of my own research, except where otherwise acknowledged, and that this thesis (or any part of the same) has not been submitted for a higher degree to any university or institution.

  
Signed:.....  
Inas Aref Saleh Naser

Date: 10/10/2004

## **ACKNOWLEDGEMENT**

I would like to express my profound gratitude to my research advisor Prof. Dr. Abdelkarim Saleh for his guidance and continuous

support through all stages of this work. My thanks will be extended to the faculty and staff members of the physics department of AL-Quds University for their help and support during my graduate work. Also, I would like to express my deep appreciation, thanks to my family, my father, my mother and all of my brothers and sisters for their continuous help, and support during the course of my graduate study. Also I would like to thank Prof. Haase of physics department North Carolina State University (NCSU), USA, for allowing Dr. A. M. Saleh to use the facilities of his lab for electrical measurements. My thanks are also extending to Prof. Renk of Regensburg University (Germany) for X-ray measurements.

Inas

Naser

ii

بِسْمِ اللَّهِ الرَّحْمَنِ الرَّحِيمِ

(...يَرْفَعُ اللَّهُ الَّذِينَ آمَنُوا مِنْكُمْ وَالَّذِينَ أُوتُوا الْعِلْمَ دَرَجَاتٍ وَاللَّهُ بِمَا تَعْمَلُونَ خَبِيرٌ)

(المجادلة، 11)

## *Dedication*

*To my father: Aref Naser*

*To my mother: Rasmeia  
Naser*

*To my grandmother: Wasfia Naser*

*To my aunt: Haifaa' Naser*

iii

## **Abstract**

A systematic study of the vortex states of  $\text{Bi}_2\text{Sr}_2\text{CaCu}_2\text{O}_x$  thick tape was carried out in the temperature range of 4 - 300 K. The tapes were grown on MgO single crystal, silver foil, or MgO coated with thin Ag-

layer. The temperature dependence of the electrical resistivity in the vortex state was found to behave according to Arrhenius like relation as:  $\rho(T) = \rho_0 \exp(-U_0/k_B T)$ , where  $U_0$  is the activation energy with values ranged between 10 and 200 meV. The activation energy is found to depend on both applied field and the growth conditions of the sample. In addition, the activation energy was found to decrease by increasing the applied field.

The current dependence on the voltage in the vortex state may be expressed by a relation  $I \sim V^\beta$ , where  $\beta$  is an exponent parameter whose values ranges between 0.5-1 depending on growth conditions and applied fields. The current was found to decrease by increasing the magnetic field at constant voltages according to the following power relation:  $I(B) \sim e^{-cB/B^*}$ . The general dependence of current on applied fields and voltages can be written as:

$$I \sim V^\beta e^{-cB/B^*}$$

The I-V characteristics were found to depend on magnetic field, voltage, heat treatment, and growth conditions.

v  
ملخص

تعني هذه الدراسة بدراسة سلوك الخصائص الكهربائية، لكل من الحالة العادية، و الحالة المختلطة، و الحالة الفائقة التوصيلية للشرائح السميكة من مادة  $\text{Bi}_2\text{Sr}_2\text{CaCu}_2\text{O}_x$ ، و اعتمادها على طريقة المعاملة الحرارية، و نوعية القاعدة التحتية (المفترض)، و المجال المغناطيسي، عند درجات حرارة تتراوح بين 300 K - 4. و عند فحص المقاومة النوعية للحالة المختلطة لهذه المادة وجد أنها تتغير وفقا لقانون (علاقة) أرهينيوز Arrhenius التي تعطى بالمعادلة التالية:

$$\rho(T) = \rho_0 \exp(-U_0/k_B T)$$

حيث أن  $U_0$  تمثل الطاقة المنشطة، و التي قيمتها تتراوح بين  $10 - 200 \text{ meV}$ . قد دلت الدراسة أن الطاقة

المنشطة تعتمد على المجال المغناطيسي، إذ وجد أنها تقل عند زيادة شدة المجال المؤثر. بالإضافة إلى ذلك فإنها تعتمد

أيضا على ظروف إنماء العينة.

و في هذه الدراسة تم أيضا دراسة اعتماد التيار على الجهد الكهربائي للحالة المختلطة للمركب، و قد وجد أن

هذه العلاقة بين التيار و فرق الجهد يمكن تمثيلها بالمعادلة التالية:

$$I \sim V^\beta$$

حيث أن  $\beta$  معامل قيمته تعتمد على ظروف إنماء العينة، و على المجال المغناطيسي المؤثر. أما علاقة التيار مع المجال،

فقد وجد أن التيار عند جهد ثابت يقل مع ازدياد تأثير المجال وفقا للعلاقة التالية:

$$I(B) \sim e^{-cB/B^*}$$

و بشكل عام يمكن أن يمثل اعتماد التيار الكهربائي على الجهد، و المجال المغناطيسي، بالعلاقة التالية:

vi

$$I \sim V^\beta e^{-cB/B^*}$$

بالإضافة لذلك و بشكل عام، فقد وجد أن ظروف المعاملة الحرارية، و ظروف إنماء الشريط و نوعية المفترش

(القاعدة التحتية) لهم تأثير كبير على مميزات (خصائص) التيار-الجهد.

**Table of contents**

**Section**

**Page**

**No.**

**No.**

**Declaration**

**i**

**Acknowledgment**

ii

**Dedication**

iii

**Abstract**

iv

**Arabic**

**Abstract**

vi

**Table of contents**

vii

**List of figures**

x

**Chapter One: Introduction and general considerations**

1.1 Introduction

1

1.2 High- $T_c$  superconductors

6

1.3 The general structure and properties of bismuth, strontium, Calcium, copper oxide (BSCCO) superconductors

8

**Chapter Two: Theoretical Review**

2.1 Introduction

10

2.2 General review

12

2.3 Dependence of electrical parameters on magnetic field  
17

2.4 The influence of the growth condition on the electrical  
properties of  $\text{Bi}_2\text{Sr}_2\text{CaCu}_2\text{O}_x$  thick tapes

21

viii

### **Chapter Three: Experimental consideration for data measurements**

3.1 Introduction

26

3.2 Preparation of the Bi-2212 tapes

26

3.3 The heat treatment profile

27

3.4 X-ray diffraction

29

3.5 Measurements

31

3.5.1 The resistivity measurements

31

3.5.2 The susceptibility measurements

32

3.5.3 The current-voltage measurements

32

3.5.4 The critical current measurements

33

3.6 Effect of growth conditions on electrical parameters

34

<b>Chapter Four: Results and discussion</b>		35
<b>Chapter Five: Summary and future work</b>		61
<b>References</b>		63
<b>Appendix A</b>		70
<b>Appendix B</b>		71
<b>Appendix C</b>		73

## List of figures

Figure  
Page  
No.  
No.

2 **Figure 1.1:** Loss of resistance of a superconductor at low temperatures.

**Figure 1.2:** The phase diagram of a superconductor, showing the

3 variation of critical magnetic field with temperature.

4 **Figure 1.3:** The variation of critical current with applied magnetic field strength.

**Figure 1.4:** a) Type-1 superconductor and b) Type-II superconductor. 5

**Figure 1.5:** Schematic plot of the crystallographic Bi-2212 tetragonal structure  
9 showing the location of the different atoms in the unit cell.

**Figure 2.1:** The variation of resistance with temperature of BSCCO system  
as observed by Maeda and coworkers (1988).

12

**Figure 3.1.** Typical heat treatment profile for partial-melts solidified  
28 Bi-2212 thick tape.

**Figure 3.2:** a) X-ray diffraction pattern of Bi-2212 sample grown on silver  
substrate. The reflected lines exhibit (001) orientation. b) The  
rocking curve of (0012) peak.

30

x

**Figure 3.3:** Illustration of the standard four-probe resistance measurement  
technique.

31

**Figure 3.4:** Determination of  $I_c$  from a typical current-voltage characteristic  
for BSCCO thick tape. 33

**Figure 4.1:** The real part of ac susceptibility of Bi-2212 thick tape sample. 36

**Figure 4.2.** A linear fit of ac susceptibility with inverse of temperature. 38

**Figure 4.3:** The resistance as a function of temperature for BSCCO thick tape (sample 46). 39

**Figure 4.4:** The logarithmic resistance ( $\ln R$ ) dependence on inverse of 40 temperature ( $1/T$ ) for thick tape sample at different fields.

**Figure 4.5:** a) A typical dependence of resistivity of the normal state on the applied magnetic field, while b) shows the effect of magnetic field 43 on the mixed state for the same sample.

46 **Figure 4.6:** Temperature dependence of the resistance first derivative.

**Figure 4.7:** Temperature dependence of the resistance second derivative for 47 BSCCO thick tape sample.

xi

**Figure 4.8:** Temperature dependence of the transport critical current for 48 Bi-2212 laser cut sample.

**Figure 4.9:** a) The critical current density  $J_c$  versus applied magnetic field for two different Bi-2212 bulk samples, and b) A semi log plot of  $J_c$  versus the applied magnetic field for the same two samples in Figure 50 4.9a with a linear fit.

**Figure 4.10:** The effect of heat treatment conditions and silver on the critical current density of Bi-2212 thick tapes. a) The sample grown on MgO substrate covered by  $1\mu\text{m}$  silver layer, and b) The sample 53 covered by  $0.5\mu\text{m}$  silver layer. grown on MgO substrate

**Figure 4.11:** A typical current-voltage characteristics curve (IVC) of 54 Bi-2212 superconductor thick tape.

**Figure 4.12:** I-V characteristics in log-log scale for a) same sample grown at zero magnetic fields at different temperatures b) for different samples grown under different growth conditions.

**Figure 4.13:** I-V characteristics in log-log scale of quenched-annealed Bi-2212 thick tape sample in various magnetic fields at different temperature.

xii

**Figure 4.14:** Dependence of current on applied magnetic field in log-log scale at different fixed voltages for Bi-2212 thick tape.

**Figure 4.15:** I-V characteristics for two different samples, grown under different heat treatment conditions for (a) a quenched-annealed sample (b) only quenched sample.

## Chapter One

### Introduction and general considerations

#### 1.1 Introduction.

Superconductivity is that state of matter, which appears in certain, metals, alloys, and compounds when cooled below a certain temperature called the transition temperature,  $T_c$ .

Onnes first observed such phenomena in 1911 when studying electrical resistance of various metals such as mercury (Hg), lead (Pb) and tin (Sn). Onnes observations confirmed that resistivity of these metals disappeared completely when the temperature was lowered below the transition temperature (Rose-Innes, 1994). The complete disappearance of the resistance of the specimen is most sensitively demonstrated by experiments with persistent currents in superconducting rings. This temperature differs from one element (or compound) to another, and it was found to decrease as the average isotope mass increases (Poole *et al.*, 1988).

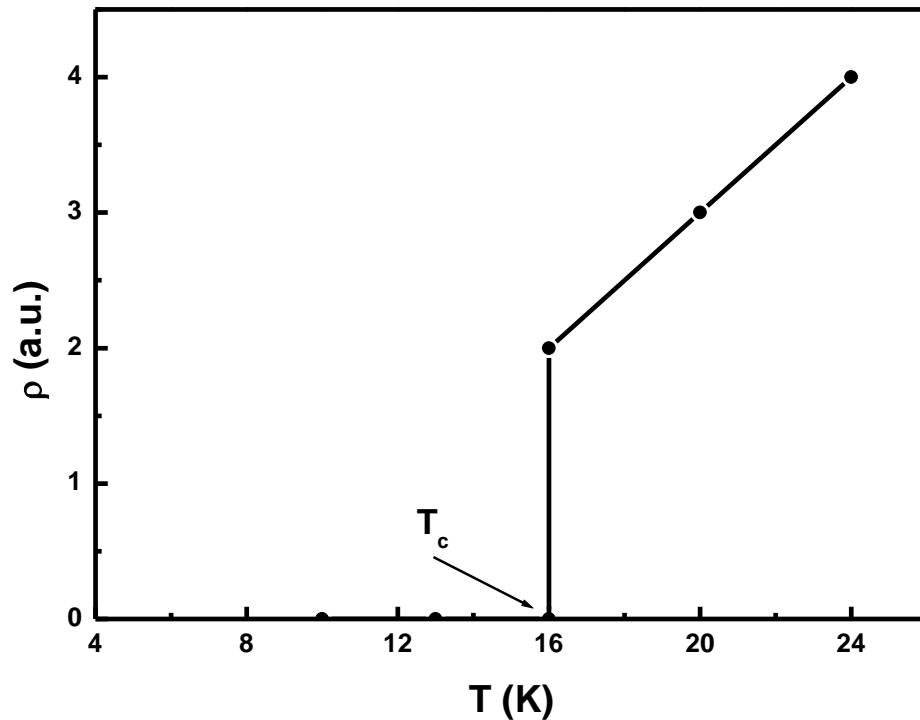


**Figure 1.1:** Typical resistivity dependence on temperature for a certain superconductor.

One of the most fundamental properties of superconductors is the so-called Meissner effect, in which the magnetic flux originally present in normal state is ejected from the bulk specimen when cooling below  $T_c$ . The superconductivity might be destroyed, if sufficient and strong magnetic fields were applied. The threshold or critical value of the applied magnetic field  $H_c$ , sufficient for the destruction of superconductivity as a function of temperature, is defined through the relation:

$$H_c = H_c(T) \quad (1.1)$$

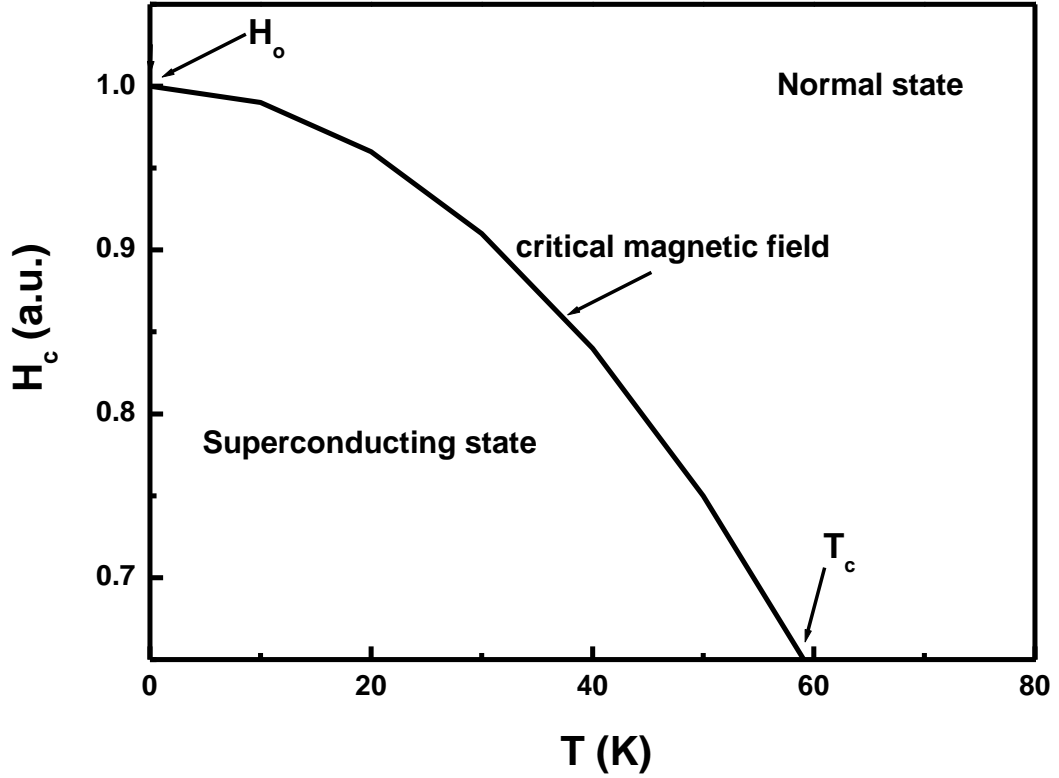


**Figure 1.2:** The phase diagram of a superconductor showing the variation of critical magnetic field with temperature.

There should be an upper limit to the amount of current flow through a superconductor in order to remain resistanceless. This current is known as the critical current,  $I_c$ . If the current exceeds this value, some resistance appears and the material reverts to normal state. For a cylindrical specimen,  $I_c$  is related to  $H_c$  through a relation (Rose-Innes, 1994):

$$I_c(T) = 2\pi a H_c \quad (1.2)$$

where  $a$  is the radius of a cylindrical wire.

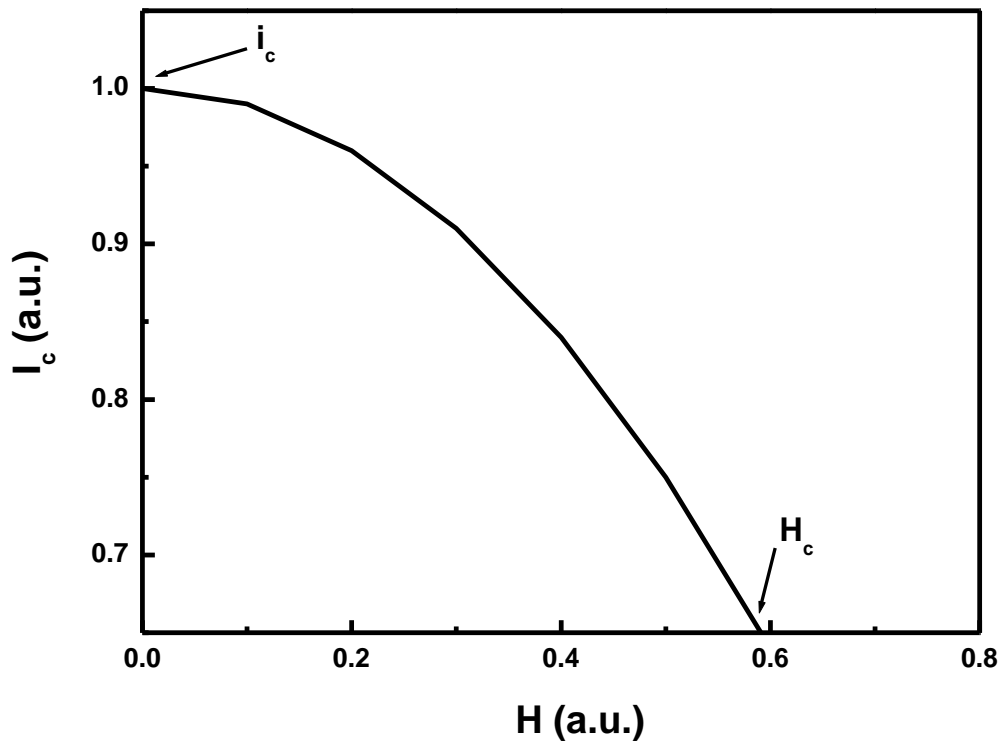


**Figure 1.3:** The variation of  $I_c$  with applied magnetic field strength.

There are two kinds of superconductors known as type-I and type-II. Most of pure elements exhibit the type-I characteristics, whereas alloys, compounds and ceramics are generally exhibit type-II characteristics. The two types have too many properties in common but they have shown considerable differences in the presence of magnetic fields (Kittel, 1996).

The mixed (or vortex) state is a region in type-II superconductors in which the material might split into some fine-scale mixture of superconducting and normal regions whose boundaries lie parallel to the

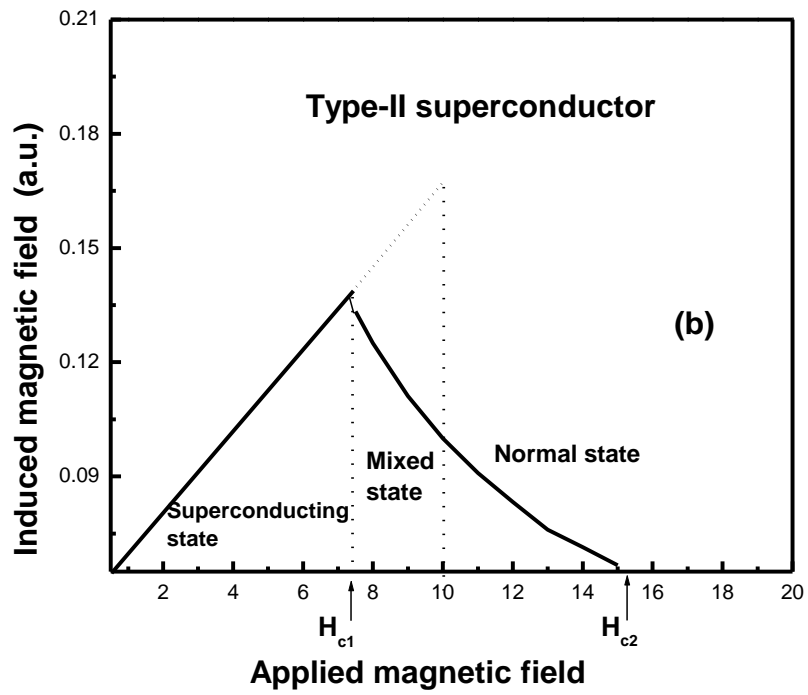
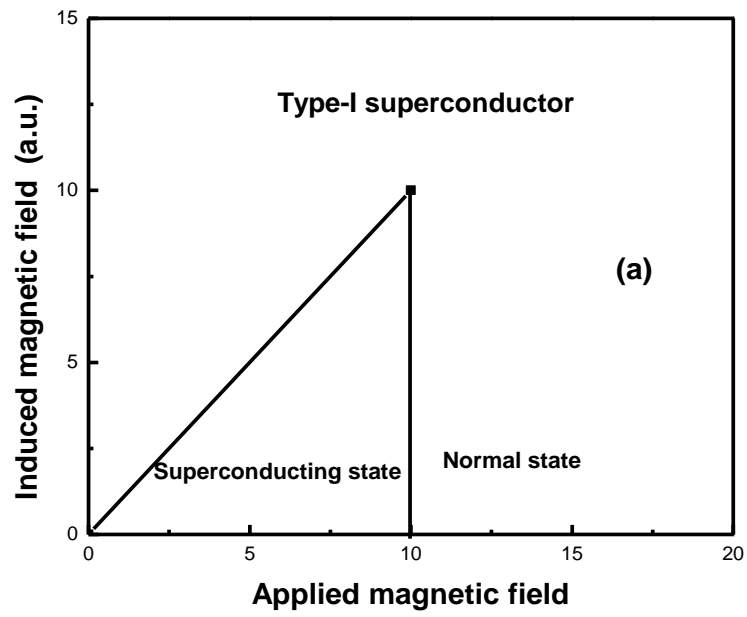


**Figure 1.4:** Typical behavior of magnetic fields on superconductors a) Type-I superconductor, b) Type-II superconductor.

applied field. Generally speaking, type-I superconductors are mainly pure metallic elements and characterized by sharp transition from normal to superconducting state, while type-II superconductors are compounds and alloys and characterized by gradual transition.

The classic 1957 papers of Bardeen, Cooper, and Schrieffer laid the basis of a quantum theory of superconductivity. The central feature of the BCS state is that the one-particle orbital are occupied in pairs, the pairs are called Cooper pairs, they have spin zero and have many attributes of bosons (Kittel, 1996).

## **1.2 High- $T_c$ superconductors.**

One of the most and important recent developments in physics of superconductors that created much excitement in the scientific community is the discovery of high-temperature (high- $T_c$ ) copper oxide superconductors, in (1987). In this case,  $T_c > 77$  K (the liquid  $N_2$ -temperature). This discovery was surprising and exciting, not simply because of the large increase in  $T_c$ , but also because it was revealed that oxides formed an unsuspected new class of superconducting materials with great scientific and technological potential (Tinkham, 1996). The new high- $T_c$  superconductors were classified into 3 main categories, namely:

1-	$\text{YBa}_2\text{Cu}_3\text{O}_7$	Y-123	$T_c = 93 \text{ K.}$
2-	$\text{Tl}_2\text{Ba}_2\text{Ca}_2\text{Cu}_3\text{O}_{10}$	Tl-2223	$T_c = 125 \text{ K.}$
3-	$\text{Bi}_2\text{Sr}_2\text{CaCu}_2\text{O}_8$	Bi-2212	$T_c = 85 \text{ K.}$

Such are superconducting ceramics categories are of extreme interest, from both scientific and from practical points of view because of their high- $T_c$  that can be achieved easily by the using the of available liquid nitrogen.

The high- $T_c$  superconducting ceramics have a layered crystal structure in general. The neighboring layers of copper oxide were separated from the next group of copper oxide layers by different layers of other metal oxides. Technically, these ceramics are not strong enough because of this layered structure. The electrical conductivity and the superconductivity properties were associated with the copper oxide planes. It was found that, the higher the number of neighboring copper oxide planes in a unit cell, the higher is the  $T_c$ . Besides, most ceramic superconductors have a very short coherence range (length  $\zeta$ ), and a very deep penetration depth ( $\lambda$ ); and they are classified as type-II superconductors. Furthermore, their superconducting properties are very anisotropic; this is because the atoms are arranged in parallel planes. That is: the properties along the **c**-axis may be widely different than those along **a** or **b**-axis.

### 1.3 The general structure and properties of bismuth, strontium, calcium, copper oxide (BSCCO) superconductors.

The first of the new families of superconductors to compete with (YBCO) is the compound of bismuth, strontium, calcium, copper oxide (BSCCO) where its superconductivity state was observed below  $\sim 114$  K. The discovery was reported on the compound  $\text{Bi}_2\text{Sr}_2\text{Ca}_1\text{Cu}_2\text{O}_x$  with a  $T_c$  of about 105 K (Meada *et al.*, 1988) and a resistive extending to 80 K before dc resistivity dropped to zero.

The family of bismuth compounds has one, two or three copper-oxygen-layers that are characterized the superconducting ceramics. The description of the structural properties of the BSCCO system is more complex than that in the YBCO. Three distinct superconducting phases have been identified in BSCCO system (Bi-2201, Bi-2212, and Bi-2223 phase) with transition temperatures of about 15 K, 85 K and 110 K, respectively. A schematic plot of the structure of the three phases belonging to the BSCCO family are shown in Appendix C. The building unit of these compounds can be written as  $\text{Bi}_2\text{Sr}_2\text{Ca}_{n-1}\text{Cu}_n\text{O}_y$ , with  $n$  equal to 1, 2, or 3 (Balastrino, 1989).

The typical tetragonal structure of the Bi-2212 system is displayed in Figure 1.5. The vectors **a** and **b** formed the base axes of the tetragonal. The primitive axes of the unit cell have dimensions of  $|\mathbf{a}| \sim |\mathbf{b}| \sim 3.8 \text{ \AA}$ , and

$|c| \sim 30.8 \text{ \AA}$ . The Bi-2212 phase has two  $\text{CuO}_2$  layers that are responsible for the supercurrent. High quality textured thin films and thick tapes could be fabricated with **ab**-plane is parallel to the substrate (Saleh *et al.*, 1997). The bismuth compounds are in general moderately ductile, resistant to chemical attack, exhibit stability in water and are fabricated easily. In addition, these compounds may be employed in several technological applications such as wires, tapes, and superconducting magnets (Doss, 1989).

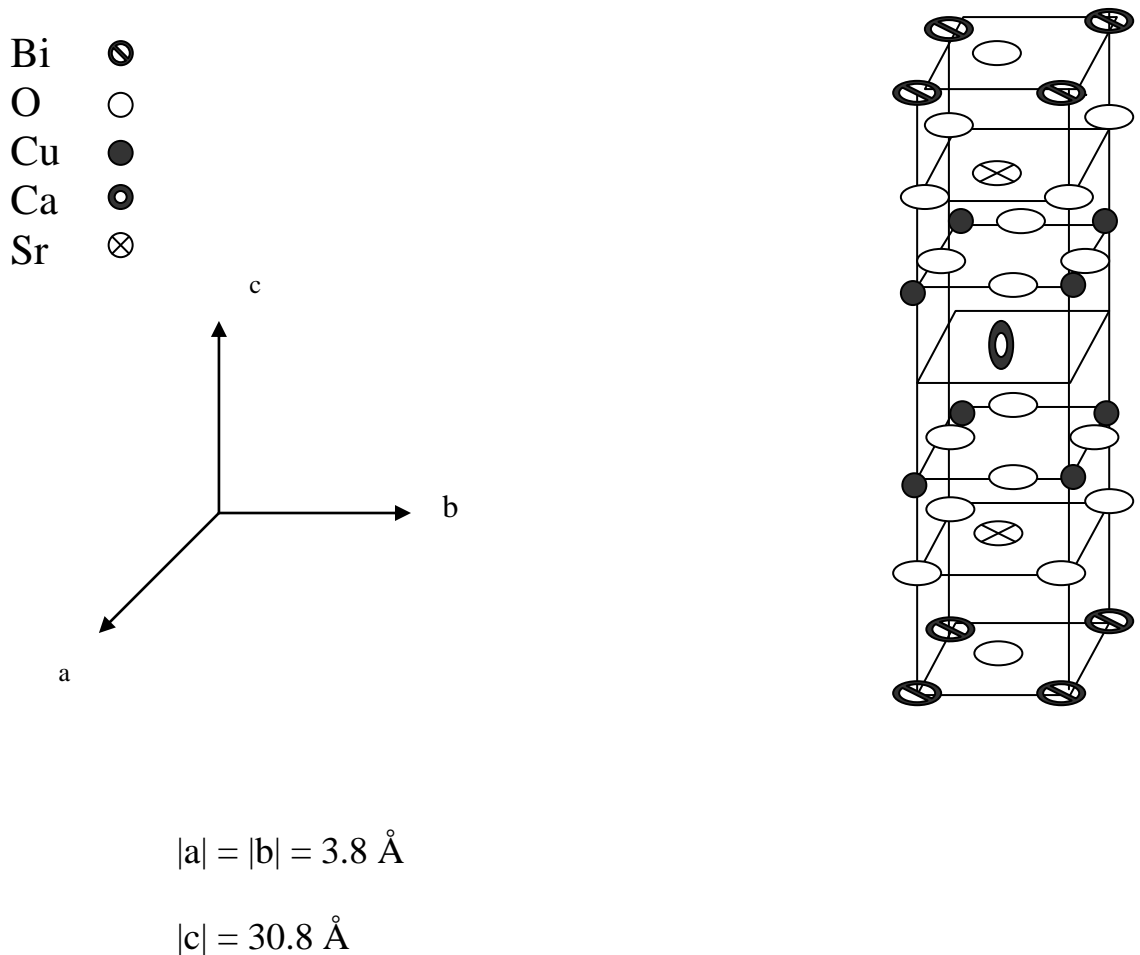


**Figure 1.5:** A schematic plot of the crystallographic Bi-2212 tetragonal structure showing the location of the different atoms in the unit cell.

## Chapter Two

### Theoretical Review

#### 2.1 Introduction

The discovery of the high- $T_c$  non-rare element superconductor Bismuth-Struntium-Calcium-Copper oxide (BSCCO) fifteen years ago by Meada and coworkers opened a new and promising era for the power and technical applications a long with scientific research using high- $T_c$  superconductors (HTSCs)(Maeda *et al.*, 1988). The transition temperature,  $T_c$ , of BSCCO oxide is about 110 K. This is higher than that of  $\text{YBa}_2\text{Cu}_3\text{O}_7$  by approximately 15 K. The coexistence of Sr and Ca in this oxide is necessary to obtain high- $T_c$  (Maeda *et al.*, 1988). The oxide is being prepared by mixing powder reagents of  $\text{Bi}_2\text{O}_3$ ,  $\text{SrCO}_3$ ,  $\text{CaCO}_3$  and  $\text{CuO}$ , and then calcined at 800 to 870 °C for several hours (~ 6 hours). Then, the mixture was thoroughly reground, cold-pressed into disk-shape pellets and then sintered at about 870 °C in air or in an oxygen atmosphere for several hours. After that the mixture is furnace-cooled or quenched to room temperature. Great effort has been employed to the syntheses of Bi-2212 or Pb doped Bi-2212 superconductor to describe the optimum conditions for the fabrication of the superconductor. Solid state reaction, partial melt, laser ablation and other techniques have been developed and

employed to fabricate the superconductor and to identify its phase diagram (Kase *et al.*; 1991; Varma *et al.*; 1989, Lee *et al.*; 1989 Holesinger *et al.*; 1993).

These oxides may have several industrial, technological and scientific fields applications. They are extremely stable, brittle in water, and moister since they are layered compounds. In addition, no change in the superconducting properties has been observed even after thermal cycling between 4 K and 300 K, even or above than that (Maeda *et al.*, 1988).

The syntheses of Bi-2212 and Bi-Pb-2212 superconductors through a novel oxide nitrate were recently described by Gibson *et al.* (2004). Mixtures of oxides nitrates, and carbonates with approximate 2:2:1:2 metal ion compositions are dissolved in HNO<sub>3</sub> and dried at 200 °C in air. The resulting superconductor contains small fraction of second phases like Bi-2201 inclusions.

## 2.2 General review.

To understand and improve the bismuth superconductor properties, it is very significant to study the electrical, magnetic, optical and structural properties of this compound. In this study we shall focus on the electrical properties. The temperature dependence of resistance for a typical high- $T_c$  superconductor compound namely BSCCO is displayed in Figure 2.1 as observed by Maeda and coworkers (1987). In this figure the Bi-2212 phase shows a metallic behavior of the resistance from room temperature to 110 K. Zero resistance is reached at about 75 K.

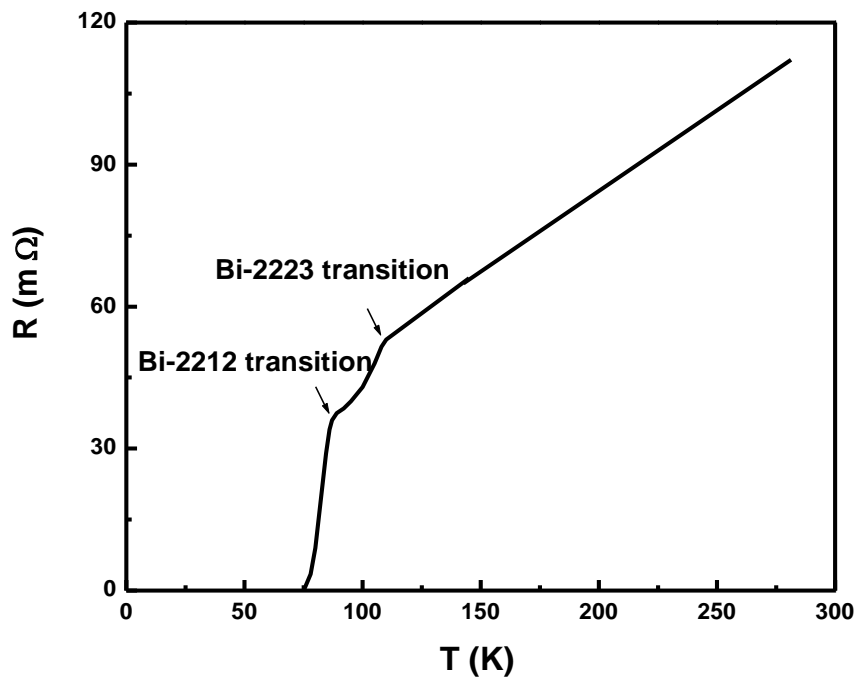


**Figure 2.1:** The variation of resistance with temperature of BSCCO system as observed by Maeda and coworkers (1988).

In most cases, devices of high- $T_c$  materials should carry high current density in order that they can be used in technological applications. The critical current density,  $J_c$ , was found to decrease by increasing the temperature. Gennes *et al.* (1964) showed for grains separated by normal material in conventional superconductor, forming superconducting-normal-superconducting (SNS) junctions. The general dependence of  $J_c$  on temperature,  $T$ , can be described by an empirical formula  $J_c \propto (1-T/T_c)^\beta$ , with  $\beta = 2$  for  $T$  close to  $T_c$ . The same behavior was reported for the high- $T_c$  phase (Bi-2223) (Marino *et al.*, 1993). It was found that  $J_c$  is about  $10^4$  A/cm<sup>2</sup> at 10 K, and its dependence on temperature follows the same power law but over a range of values between 0.03 and 0.7. This behavior indicates that, the electrical transport mechanism in Bi-2223 single-phase film is determined mainly by (SNS) junctions.

Balestrino (1989) deduced the value of the critical current density both along the **c**-direction and in the **ab**-plane. For a single crystal of the Bi-2212 phase. Values of  $5 \times 10^4$  A cm<sup>-2</sup>, and  $1.2 \times 10^6$  A cm<sup>-2</sup> along **ab**-plane, respectively at 4.2 K. The dependence of  $J_c$  on the angle between magnetic field and **c**-axis was also measured by Kumakura *et al.* (1991) for textured Bi-2212 tape at 4.2 K in magnetic fields up to 8 T. A fairly large hysteresis in  $J_c$ - $\theta$  phase diagram was obtained.

This type of hysteresis behavior is attributed to the weakness of grain coupling in the sample.

Saleh *et al.* (1998)<sup>a</sup> had studied the current-voltage characteristics IVCs for bulk and single grain boundary BSCCO samples grown under various growth conditions. The I-V characteristics for grain boundaries were scaled according to the following power relation:

$$V \propto (I - I_c)^n \quad (2.1)$$

for  $I > I_c$  with an exponent  $n$  larger than one. The curvature of the I-V curve is upward above  $I_c$ . This type of IVCs curves was also observed in a single grain or polycrystalline bridges (Zitkovsky *et al.*, 1991). Gurevich and coworkers (1993) showed that the V-I curves are nonlinear at  $I$  near  $I_c$  and become linear above the critical current,  $I > I_c$ . The nonlinearity of  $V(I)$  at small voltages in BSCCO was explained on the basis of flux creep model. Unlike the low- $T_c$  composites phase, the nonlinearity of  $V(I)$  often results from macroscopic variations of  $I_c$  along the superconducting filament (Warnes *et al.*, 1986).

Tinkham and Lobb (1989) have proposed the dual superconducting transition model for a network of weak links that connect superconducting grains. According to this model, as the superconducting transition within grains occurred, followed at lower temperature, the establishment of long-range superconducting order, or phase coherence, between grains will be

followed at low temperatures. Usually, these mechanisms were referred to as the intragranular and intergranular superconducting transition, respectively.

In an extensive set of measurements, Pekala *et al.* (1995) was observed an anisotropy in the transport properties of the textured Bi-2223 superconductor. A stronger influence of the magnetic field along the **c**-axis than along the **a**-axis has been observed. Anisotropy measurements should be carried out on single crystals; since the sample is uniform along each axes with no boundaries and cracks or impurities. Resistivity measurements on single crystals have shown that along **c** direction,  $\rho_c$ , is much larger than the **ab**-plane resistivity,  $\rho_{ab}$ , (Martin *et al.*, 1989). At the transition temperature, the resistivities ratio  $\rho_c/\rho_{ab}$ , is about  $10^5$ . Such result is in agreement with the high structural anisotropy of these compounds and with the idea that related to superconducting  $\text{CuO}_2$  planes.

Chakrabarti *et al.* (2003) were studied the anisotropy of the electron momentum distribution in Bi-2212 superconductor by positron annihilation. The general behavior for the electron momentum distribution has been found to have a larger value along the crystallographic **c**-axis than in the **ab**-plane throughout the temperature range from 30 to 300 K.

Grader *et al.* (1988) proposed unit cell formula for the Bi-2212 phase, that can be written as  $\text{Bi}_2\text{Sr}_{3-x}\text{Ca}_x\text{Cu}_2\text{O}_{8+\delta}$  with  $x$  varies between 0.8

and 2.2. The lattice parameters of the Bi-2212 compound decrease monotonically with increasing  $x$ . In addition, Shaimoyama *et al.* (1992) were studied the oxygen nonstoichiometry  $\delta$  of Bi-2212 and its dependence on thermodynamic quantities, lattice constant and critical temperature. Anomalous behaviors of such quantities in the dependence on  $\delta$  at  $\delta = 0.235$  has been observed. This is an indicates of the possibility existence of two phases in Bi-2212 compound due to this anomaly.

From thermo-gravimetric measurements and neutron diffraction studies, the effect of non-stoichiometric oxygen on  $T_c$  has been also observed in the BSCCO system (Pena *et al.*, 1989). An oxidizing atmosphere was found to reduce  $T_c$  and to increase the superconducting transition width. Systematic studies were performed for Bi-2212 in the range  $8 < y < 8.30$ , where  $y$  is the oxygen index. This can be achieved by annealing of the highly oxidized single-phase powders under inert atmosphere in order to remove oxygen in small steps. Heating treatment was performed at temperatures between 300 and 750 °C for 24 h in order to attain equilibrium between oxygen contents in samples. This is resulted in a dramatic decrease of  $T_c$  in connection with the high oxygen contents observed in Bi-2212 (Bock *et al.*, 1990).

Ishizuka *et al.* (1990) had confirmed that regulating the activated oxygen flux density control the crystalline orientation of BSCCO thin films. Two orientations were observed, one when the  $c$ -axis is oriented

perpendicularly to the film surface and the other when the c-axis is inclined about 50 degrees from the perpendicular to the film surface.

### **2.3 Dependence of electrical parameters on magnetic field.**

Electrical and magnetic properties of HTSCs are greatly affected by the application of magnetic field. When the applied magnetic field is equal to zero, the resistive transition is nearly sharp, while in the presence of magnetic field the resistive transition is rather broad and develops a large tail. This behavior was observed when the magnetic field is perpendicular to the c-axis in thin films or thick tapes. The broadening becomes more significant, particularly, in the low resistance portion. A tail in the resistance profile was observed over the wide temperature range for both directions (parallel and perpendicular to c-axis) of magnetic fields (Kobayashi *et al.*, 1989). In this region, the flux flow resistance will be added to the normal resistance, therefore shifting  $T_c$  to left (lower temperature). Moreover, by increasing the magnetic field, the resistivity shifts to lower temperatures as expected for granular superconductor. This same behavior was observed in single crystals of BSCCO and thick tapes (Plastra *et al.*, 1989). As pointed out by Maeda *et al.* (1991), the appearance of the finite resistance under the magnetic field is mainly

attributed to the large fluctuation effect, which leads to resistive broadening.

A profound look to the dependence of resistivity on magnetic field in the transition region is achieved by studying the transition region in terms of the derivative curves ( $dR/dT$ ). Two peaks were observed in the plots of the temperature derivative of the resistance, ( $dR/dT$  versus  $T$ ) (Goldschmidt 1989, Nkum and Datars 1995). The major peak corresponds to intra-granular transition, while the secondary peak corresponds to inter-granular transition. The latter peak is broadened as the bias current or the magnetic field strength is increased and shifts to lower temperatures.

The critical current density of the superconducting state is extremely dependent on the applied magnetic field especially at high temperatures. Togano *et al.* (1991) found that  $J_c$  decreases rapidly as the magnetic field strength increased above  $T > 30$  K. However, below 30 K, the critical current density  $J_c$  was found to vary slowly with fields even for high field strength up to 25 T (Togano *et al.*, 1991, Kase *et al.*, 1991, Shimoyama *et al.*, 1992). Kumarkura *et al.* (1991) had observed large decrease in  $J_c$  as the field increased above 25 K and its anisotropy became very large. This indication that flux pinning is effective only for cases in which the flux is perpendicular to the axis where flux vortices can move easily within the **ab**-plane. On one hand, Gurevich *et al.* (1993) showed

that  $J_c(B)$  decreases as  $B^{-0.15}$  for the Bi-2212 tape at 4.2 K, and on the other hand, the  $J_c(B)$  dependence becomes exponential at 77 K.

At temperatures above 30 K, the application of magnetic fields up to 8 mT had a little effect on the shape of IVC curves (Saleh *et al.*, 1998). At low temperatures, the hysteresis in IVC curves is believed to be typical in HTSC material especially in the Bi-based sample. This behavior may be attributed to the weak coupling between grains through Josephson junction (Kleiner *et al.*, 1994). In addition, it was found that the highly layered of Bi-2212 gives rise to intrinsic Josephson junction even in single crystals.

The susceptibility measurement is a powerful tool in determining valuable information about the electric and magnetic properties of the superconductor such as magnetization, critical currents, the order parameter and many other properties (Widder *et al.*, 1997). It is well established that the ac susceptibility ( $\chi = \chi' - i\chi''$ ) depends strongly on the amplitude and the frequency of the ac field ( $B = B_0 \cos \omega t$ ) of the primary coil and the applied dc field. Many researchers found that both  $\chi'(T)$  and  $\chi''(T)$  curves shift to higher temperatures as both the frequency and the peak temperature  $T_p$  (peak temperature) increase exponentially with the frequency (Saleh *et al.*, 2003, Han *et al.*, 1993). Such observation was interpreted in terms of flux creep.

The real part of the susceptibility has shown a two-step transition corresponding to the superconducting state for different dc magnetic field. The first step transition is attributed to the grain forming the specimen. This transition is almost independent of the field amplitude. The second transition is related to the intergrain regions and it is observed to be field dependent (Gonzalez *et al.*, 1995). The two step transition to the superconducting state is confirmed by measuring the resistive (imaginary) part of the susceptibility  $\chi''$ . This part represents the bulk pinning hysteresis losses in the sample due to the motion of the vortices (Josephson vortices) in and out grain boundaries (Müller *et al.*, 1989). Bi-2212 crystals showed only a single  $\chi''$  peak, which is more strongly affected by magnetic fields and the frequency of measurements than are those of  $\text{YBa}_2\text{Cu}_3\text{O}_{7-x}$  (Flippen *et al.*, 1992). Gonzalez *et al.* (1995) was observed two peaks in the imaginary part of the complex susceptibility of Bi-2223 ceramic superconductor.

Ray *et al.* (2002) used the field dependence of real ( $\chi'$ ) and imaginary ( $\chi''$ ) component of ac susceptibility of (Bi-Pb)-2223 superconductors within the critical state model to evaluate and study the temperature dependence of intergranular critical current density of polycrystalline near  $T_c$ . They found that the intergranular  $J_c$  (0 K) has values vary between  $2.23 \times 10^5 \text{ A/cm}^2$  and  $2.3 \times 10^5 \text{ A/cm}^2$  for sample with densities  $5.39 \text{ gm/cm}^3$  and  $5.86 \text{ gm/cm}^3$ , respectively. This result in

agreement with the fact that in polycrystalline HTSCs the critical current is primarily dominated by weak links.

#### **2.4 The influence of the growth condition on the electrical properties of $\text{Bi}_2\text{Sr}_2\text{CaCu}_2\text{O}_x$ thick tapes.**

The electrical parameters of the normal, the vortex, and the superconducting state of BSCCO are affected greatly by the growth conditions. Several factors were found to limit  $J_c$ ,  $T_c$  and other properties of the Bi-2212 thick tapes were found to depend on several factors among, such as grain boundaries, defects, and second phases, ...etc, (Yang *et al.*, 1992). Samples of large grain size and grown from melt have shown higher  $T_c$  and higher  $J_c$  than those samples of small grains (Lee *et al.*, 1991). The differences in superconducting properties between these samples were attributed to the crystal growth conditions and weak-link behavior at grain boundaries.

The type of substrate material was found to be very critical in the formation of the superconducting phase under partial melting growth technique. Silver foil, single crystal MgO and MgO coated with thin silver layer were good environments for the formation of Bi-2212 superconducting phase (Saleh *et al.*, 1997). Silver was found to play an important role in grain alignment and the formation of highly textured

microstructure (Kase *et al.*, 1991). In addition, the amount of silver added to the sample has a strong influence on  $J_c$  at 77 K (Kobel *et al.*, 2003). Fujishiro *et al.* (1993) has pointed that alloying Ag with Au or Cu decreases the thermal conductivity relative to pure Ag. The additions of Au were greatly effective in decreasing the thermal conductivity. Nomura *et al.* (1993) has studied the influence of Au or Cu additions to the Ag substrate on the microstructure and properties of the Bi-2212 superconductors. They found that Bi-2212 prepared on an Ag-Au substrate showed excellent  $J_c$  values. In addition, they expected that Ag-Au alloy to be superior substrate materials of Bi-2212 for power current lead in superconducting magnets, taking into account their low thermal conductivity.

Heat treatment conditions also affected the electrical parameters of the Bi-2212 superconductor. Noji *et al.* (1993) was found that the growth of second phases on the tape surfaces is dependent on the cooling rate from the sintering temperature all the way down to room temperature. In addition, they found that the grain boundaries depend on the cooling rate and this was related to the morphology of the sample surface. Moreover, Shiomyama *et al.* (1992) was found that a fast cooling rate would suppress the decomposition of the Bi-2212. And thus the grain coupling of the superconductors will be improved and hence increasing  $J_c$ . Besides,

$T_c$  was found to decrease with decreasing the cooling rate (Noji *et al.*, 1993).

Furthermore, the superconductor properties of BSCCO tape were found to depend on annealing and sintering temperatures, time of heat treatments and the furnace atmosphere (Dimesso *et al.*, 1992). Also, observations have shown that annealing under reducing atmosphere on BSCCO textured tapes and for different time periods could vary  $T_c$ . Besides,  $J_c$  was affected greatly by the annealing due to the degradation of the interface at the grain boundaries. Natividad *et al.* (2004) analyzed the changes produced within the bulk Bi-2212 along thermal treatment (annealing) and the subsequent cooling to room temperature. Accordingly, the different stages of the thermal process, the samples present different degrees of homogeneity in their superconducting properties.

Kobel *et al.* (2003) observed three regions for the dependence of  $J_c$  on the maximum processing temperature (895 - 905 K). Firstly, the region in which  $J_c$  rises slowly with increasing maximum process temperature up to 20 °C above the solidification temperature. Secondly, at temperatures between 25 - 30 °C and above the solidification temperature, the highest  $J_c$  values were attained. Thirdly,  $J_c$  decreases rapidly with further increasing processing temperatures.

The electrical and magnetic properties of Bi-2212 system were being greatly affected by the type of dopant. Prabhu *et al.* (1993) studied the influence of Fe and Co on the Bi-2212 phase transition. It was found that by increasing dopant concentration, a systematic decrease in  $T_c$  would be followed. Susceptibility also indicated a decrease in the volume fraction of the doped phases. Moehlecke *et al.* (1993) studied the effect of Li addition on the Bi-2212 compounds; they found that the addition of lithium will increase the volume of superconducting material. The addition of Li enhances the superconducting properties of the weak intergranular links, making these regions more homogeneous and less sensitive to magnetic fields. Furthermore,  $T_c$  ( $T_{c \text{ intra}}$  and  $T_{c \text{ inter}}$ ) and  $J_c$  are found to increase significantly with increasing Li concentration.

Jin *et al.* (1993) studied the influence of growth conditions such as heating time, amount of Pb doping, temperature, ...etc, on the size and superconducting phase of the Bi-based grown whiskers. Whiskers are made up of several single crystal plates staking into layered structures (needle like), and they have perfectly oriented structures. Besides, they have also a very strong current carrying ability. Jin and coworkers (1993) found that the maximum length of the whiskers is proportional to the growth time at initial stages, and after a certain growth time, the maximum length stays constant. High- $T_c$  phase emerges when the growth time is prolonged for the whiskers whose starting compositions are near

the stoichiometry of the high- $T_c$  phase. The optimum temperature for the whisker growth is in a very narrow range, which is just below the melting point of the substrate. They also found that the state of the substrate had little effect on the whisker growth. In addition, the amount of Pb doped in the starting materials and a steady stream of oxygen atmosphere play catalytic roles in the whisker growth.

## Chapter Three

### Experimental consideration for data measurements

#### 3.1 Introduction.

Experimental data were collected for Bi-2212 superconductor thick tapes in the temperature range from 4 to 300 K at both North Carolina State University (USA) and Regensburg University (Germany). The main aim of the analysis of the data is to develop models able to describe the general behaviors of the system. Besides, the analysis of the data will be helpful in estimating certain electrical parameters like activation energy, mobility, Hall coefficient, etc...

In this chapter, we shall focus on describing briefly the experimental procedures used in the preparation of Bi-2212, and the methods employed in measuring electrical parameters.

#### 3.2 Preparation of the Bi-2212 tapes.

A commercial fine powder of Bi-2212 thoroughly mixed with organic formulation [trichloro-ethylene as solvent, sorbitan trifoliate as dispersant, and poly-vinyl butyral as binder] (Saleh *et al.*, 1997 and 1998<sup>b</sup>). The mixture was then cast on glass plate, using the doctor blade technique, into typically green sheet of about 125 mm-wide and 50  $\mu\text{m}$ -

thick (Togano *et al.*, 1991). Tape samples are then cut from the green tape, each sample with dimension of about  $4 \times 1 \text{ mm}^2$ , are placed on a substrate (Saleh *et al.*, 1998). Several substrates were used such as: silver foil of thickness of  $50 \text{ }\mu\text{m}$ , MgO single crystal, and MgO single crystal coated with a silver layer of about  $0.5 - 1 \text{ }\mu\text{m}$  thickness. After the preparation, the sample was subject to heat treatment to obtain a superconductor. Various heat treatment conditions were employed for the different samples to examine their effect on the properties of the superconductor.

### **3.3 The heat treatment profile.**

Figure 3.1 shows a profile of typical heat treatment used for sample growth. Firstly, to remove the organic formulation, the composite tape was heated slowly to  $500 \text{ }^\circ\text{C}$  and kept at that temperature for two hours. Secondly, the temperature was raised to either  $890$  or  $900 \text{ }^\circ\text{C}$ , depending on the substrate material, (the temperature was raised to  $890 \text{ }^\circ\text{C}$  for Ag substrate, or  $900 \text{ }^\circ\text{C}$  for MgO substrate). At this temperature, a partial melting of the oxide was obtained and the sample is left for about 10 minutes. Thirdly, the temperature is slowly cooled at a rate of  $0.1 \text{ }^\circ\text{C}/\text{min}$  to  $840 \text{ }^\circ\text{C}$ ; the sample was then kept at this temperature for 6 hours. Fourthly, the sample is either quenched or slowly cooled to room

temperature at different rates. The final oxide thickness was about 12 - 20  $\mu\text{m}$ , which is about 25 to 33 % of the initial green tape thickness.

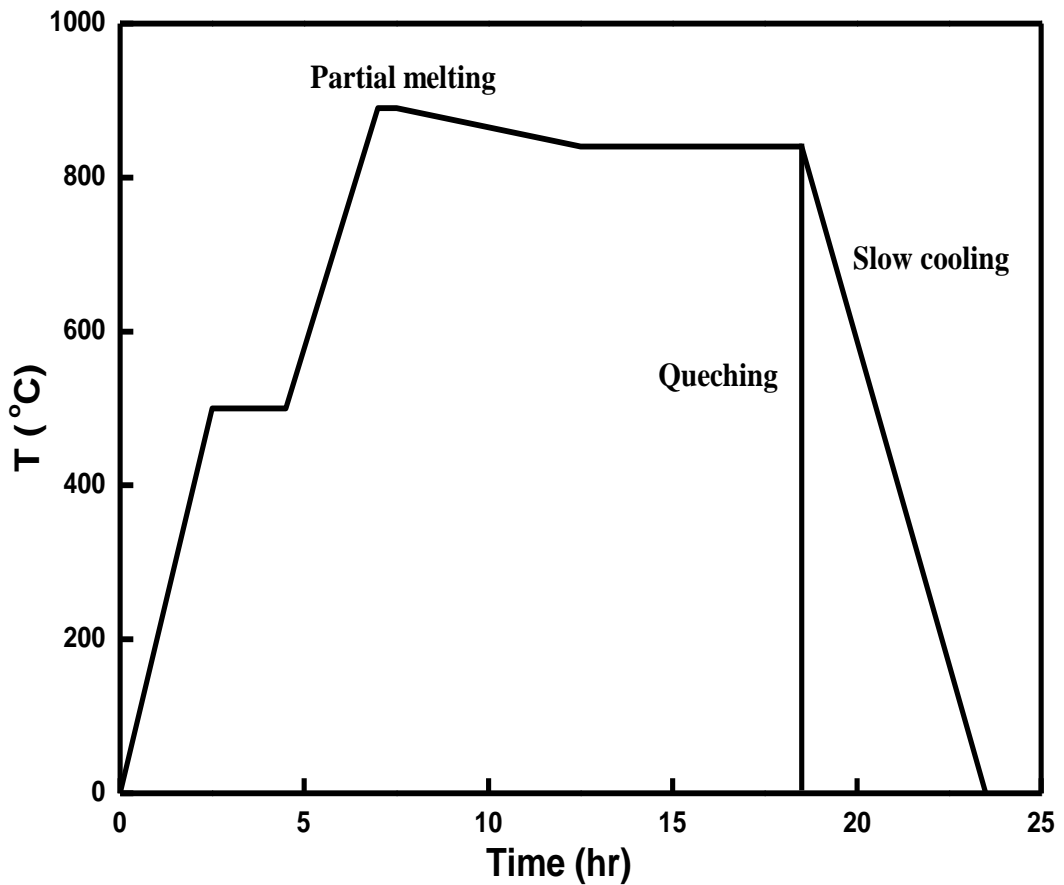


**Figure 3.1:** A typical heat treatment profile for partial- melts solidified Bi-2212 thick tape.

### 3.4 X-ray diffraction.

To check the composition and the alignment of the grains (sample) on the substrate, X-ray diffraction (XRD), was performed on some samples. A Seifert XRD 3000R diffractometer using  $\text{Cu}_{k\alpha}$  radiation was utilized for X-ray investigation. Figure 3.2a shows a typical X-ray diffraction pattern of Bi-2212 sample grown on silver substrate. The c-axis orientation of the grains is almost perpendicular to the substrate as confirmed by the X-ray diffraction profile, which predominantly exhibit (00l) peaks. The small peaks assigned by \* on the graph are due to (hk1) reflection lines. To confirm the alignment of the grains, rocking curves were also taken for some samples. In this case, we select a certain peak (00l) and XRD reflection was taken around it in  $360^\circ$ . From such rocking curve, we can determine the degree of disorientation of the c-axis oriented grains. Figure 3.2b demonstrates as an example of the rocking of the (0012) peak. The full width at half maximum (FWMA) of this peak is approximately  $8^\circ$ , indicating a reasonably well-oriented c-axis specimen. It is worth to note that the FWMA in epitaxial film growth is typically  $1^\circ$  (Saleh *et al.*, 1998<sup>b</sup>).

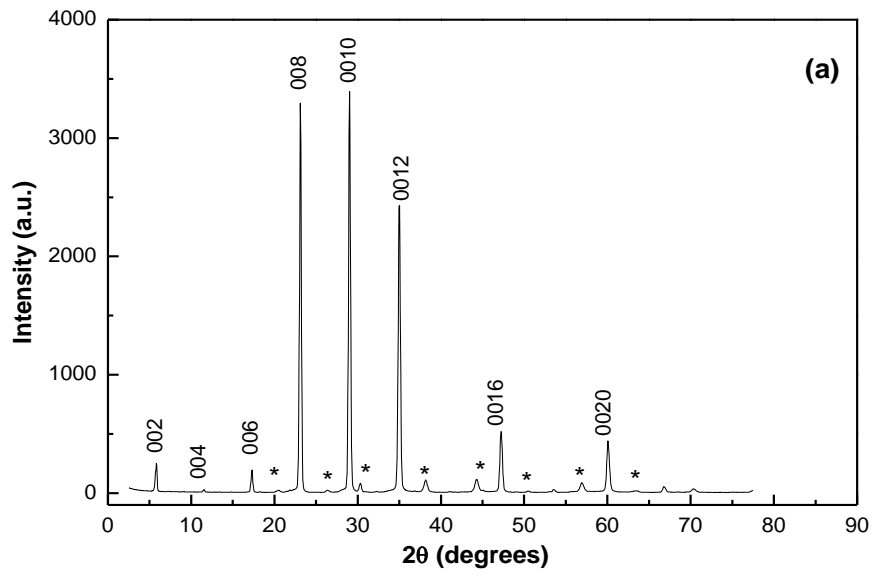


**Figure 3.2:** a) X-ray diffraction pattern of Bi-2212 sample grown on silver substrate where the reflected lines exhibit (001) orientation, and b) The rocking curve of (0012) peak.

### 3.5 Measurements.

#### 3.5.1 The resistivity measurements.

The superconducting behavior of a sample could be confirmed by measuring the resistivity of the material and the AC susceptibility. A standard four-probe technique was employed for the resistivity measurements. This technique employs two leads (or probes) to measure the current flowing in the sample,  $I$ ; while the other two leads measure the potential drop,  $V$ , between two equi-potential surfaces resulting from the current flow. A sketch of the four-probe technique apparatus is displayed in Figure 3.3. The resistance of samples with dimension of about  $6 \times 2 \times 0.02 \text{ mm}^3$  were measured in the temperature range 80 to 150 K with or without external field parallel to the  $c$ -axis. Gold leads were attached to the sample using silver paint.

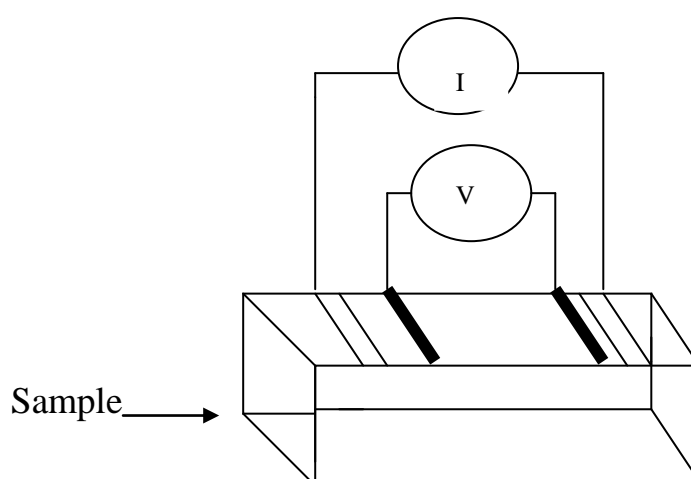


**Figure 3.3:** Illustration of the standard four-probe resistance measurement technique.

### **3.5.2 The susceptibility measurements.**

The Ac and Dc susceptibilities are measured using a standard homemade susceptometer with a standard lock-in amplifier. The susceptometer consists of a primary coil and two identical pick-up coils, one of them surrounding the sample. In the Ac measurements, the susceptibility is measured for samples of dimensions of  $2 \times 2 \times 0.02 \text{ mm}^3$  for various fields of different amplitudes and frequencies. The measured voltage,  $V$ , in the lock-in amplifier (in-phase and out-of-phase voltage) is directly proportional to the susceptibility through the relation:  $\chi \propto V/H_0$ , where  $H_0$  is the magnetic field produced by the current in the primary coil. The in-phase voltage gives the real part of  $\chi$ , while the out-of-phase voltage gives the imaginary part. In the dc measurements, the strength of the applied field is varied.

### **3.5.3 The current- voltage measurements.**

The current-voltage characteristics (IVCs) were taken using a current source driven by a ramp generator with a maximum output current of  $\pm 100 \text{ mA}$ . The sample was mounted on a dipstick that could be inserted in a liquid helium container. A small magnetic field up to  $8 \text{ mT}$  could be applied to the sample. In the present study, the field was applied on the sample parallel to the c-axis to study its effect on the resistivity of

the normal and vortex states and its effect on  $J_c$  and  $T_c$  of the superconducting state.

### 3.5.4 The critical current measurements.

Several methods and techniques can be used to determine  $J_c$  in superconductors. One of these methods (used in the present study) is the determination of the critical current from the IVCs with a 1- $\mu\text{V}$  voltage criterion. The average value of both ends of the curve when the voltage starts to develop across the sample was used to determine  $I_c$ . That is:

$$I_c = \frac{I_{c1} + I_{c2}}{2} \quad (3.1)$$

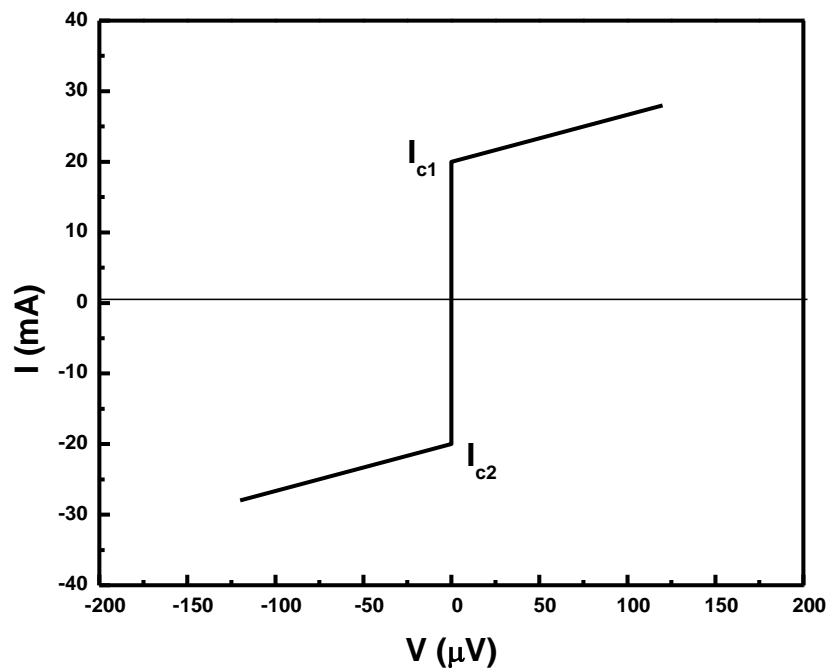


**Figure 3.4:** Determination of  $I_c$  from typical IVCs for BSCCO thick tape.

### **3.6 Effect of growth conditions on electrical parameters.**

The dependence of electrical parameters of normal, vortex, and superconducting states of BSCCO on the substrate material, heat treatment conditions and applied magnetic field were studied for partial melt-solidified superconducting tapes.

The effects of substrate material were studied by growing the samples on various types of substrates such as Ag foil (50  $\mu\text{m}$  thick), single crystal MgO and MgO substrates coated with silver layer (Saleh *et al.*, 1997). Besides, the effect of heat treatment conditions was studied by growing many samples under different heat treatment conditions. Some of the samples were annealed in a nitrogen atmosphere at 500 to 550  $^{\circ}\text{C}$  for about 14 hours and then cooled to room temperature either by quenching or slow cooling. Therefore, the effect of heat treatment-conditions, the annealing atmosphere, and the cooling rate on the electrical parameters were investigated.

## Chapter Four

### Results and Discussion

The collected data for the Bi-2212 superconducting thick tapes will be analyzed on the basis of the models discussed in chapter two. The superconducting behavior was determined by measuring Ac susceptibility and the resistivity of the material. The Ac susceptibility measurements provide a great deal of information about electric and magnetic properties of the sample and give a better indication of the extent to which the sample has transformed to the superconducting state.

The real part of the susceptibility of Bi-2212 thick tape as a function of temperature is shown in Figure 4.1. From this figure we can see the transition in the magnetic behavior for the Bi-2212 thick tape from paramagnetism to perfect diamagnetism at  $T_c = 78$  K. The same behavior was found for  $(\text{Bi,Pb})_2\text{Sr}_2\text{Ca}_2\text{Cu}_3\text{O}_y$  superconductor, prepared in a single-phase polycrystalline form (Maeda *et al.*, 1989).

The Curie law may express the magnetic susceptibility of many compounds that gives the paramagnetic susceptibility as inversely proportional to the absolute temperature  $T$ , according to the following expression (Mulary, 1963):

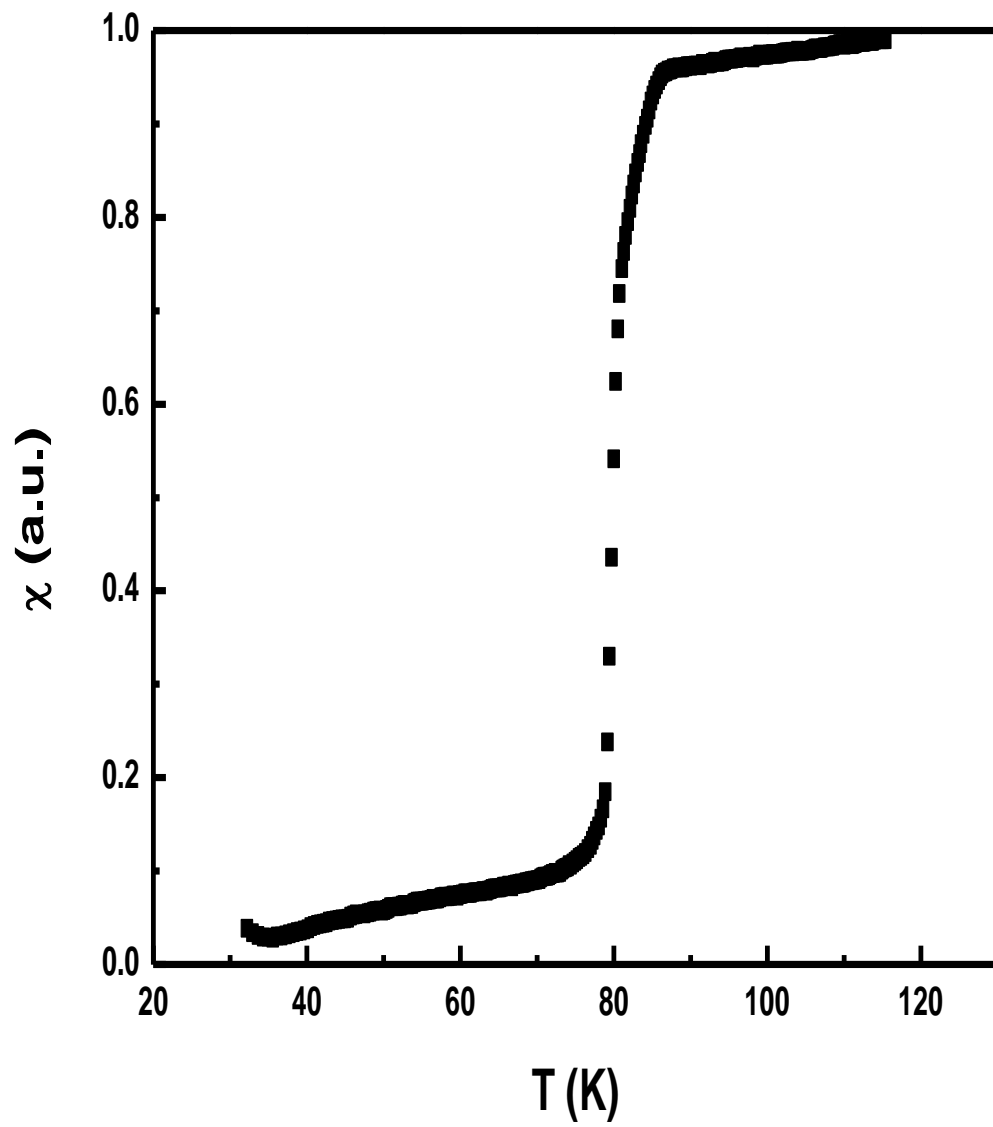


**Figure 4.1:** The real part of ac susceptibility of Bi-2212 thick tape sample

$$\chi = \frac{C}{T} \quad (4.1)$$

where  $C$  is called the Curie constant, which is equal to (Kittel, 1996):

$$C = \frac{Np^2\mu_B^2}{3k_B} \quad (4.2)$$

where  $N$  is the number of atoms per unit volume,  $k_B$  is the Boltzmann constant,  $\mu_B$  is Bohr magneton, and  $p$  is the effective number of Bohr magnetons, which may be calculated from the relation:

$$p = g [J(J+1)]^{\frac{1}{2}} \quad (4.3)$$

in Bohr magneton units. Here  $g$  is the Lande splitting factor and  $J$  is the resultant angular momentum, which is a vector sum of  $L$ , the total angular momentum of the orbital motion of the electrons, and  $S$ , the corresponding spin angular momentum (Mulary, 1963).

The linear relation between  $\chi$  and  $1/T$  for Bi-2212 bulk sample exhibited in Figure 4.2 is used to find the permanent moment  $\mu$ . The Curie constant  $C$  estimated from the slope of this figure is equal to 11.6. Using this result, we can find the permanent Bohr magneton  $\mu_B$  in terms of  $C$  by applying the relation that  $\mu_B = (3k_B C / Np^2)^{1/2}$ .

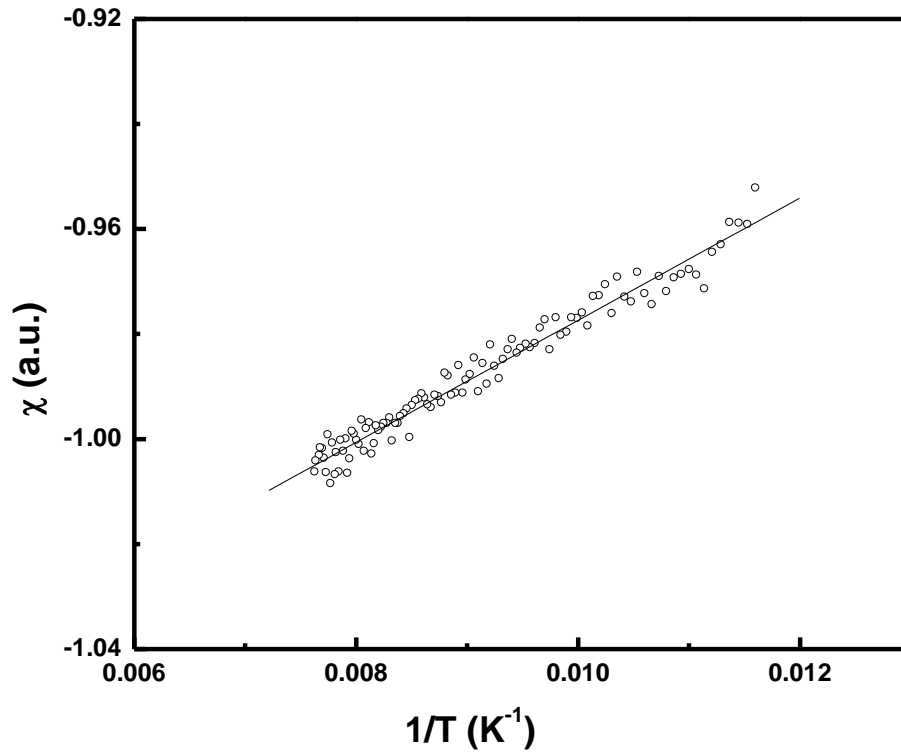


**Figure 4.2:** A linear fit of AC susceptibility with inverse of temperature.

The variation of the resistance with temperature of Bi-2212 bulk sample is shown in Figure 4.3. The sample shows a metallic behavior of the resistance from room temperature to 110 K, while zero resistance is reached at 85 K. Same behaviors for various samples of different growth conditions were observed but with different  $T_c$ . The data for different samples were plotted (Figure 4.3) and the linear part was fitted to find the temperature dependence of the resistance. The temperature dependence of the resistance is well expressed by a linear relation of the form:

$$R(T) = A + BT \quad (4.4)$$

where A is the residual resistance extrapolated to  $T = 0$  (intercept), and B is the slope. The same behavior was found for polycrystalline sample of  $\text{YBa}_2\text{Cu}_3\text{O}_7$  system (Pureur *et al.*, 1991),  $(\text{Bi-Pb})_2\text{Sr}_2\text{Ca}_2\text{Cu}_3\text{O}_x$  silver-sheated tapes (Xu *et al.*, 1997) and for  $\text{Bi}_2\text{Sr}_{2-x}\text{Gd}_x\text{Ca}_1\text{Cu}_2\text{O}_{8+\delta}$  ( $x = 0 - 0.65$ ) system (Khan, 1994). Typical values of A and B for various samples are recorded in table 1. According to the table, the values of A and B are strongly dependent on the sample properties (i.e. growth conditions, annealing time and atmosphere, substrate type and grain size).

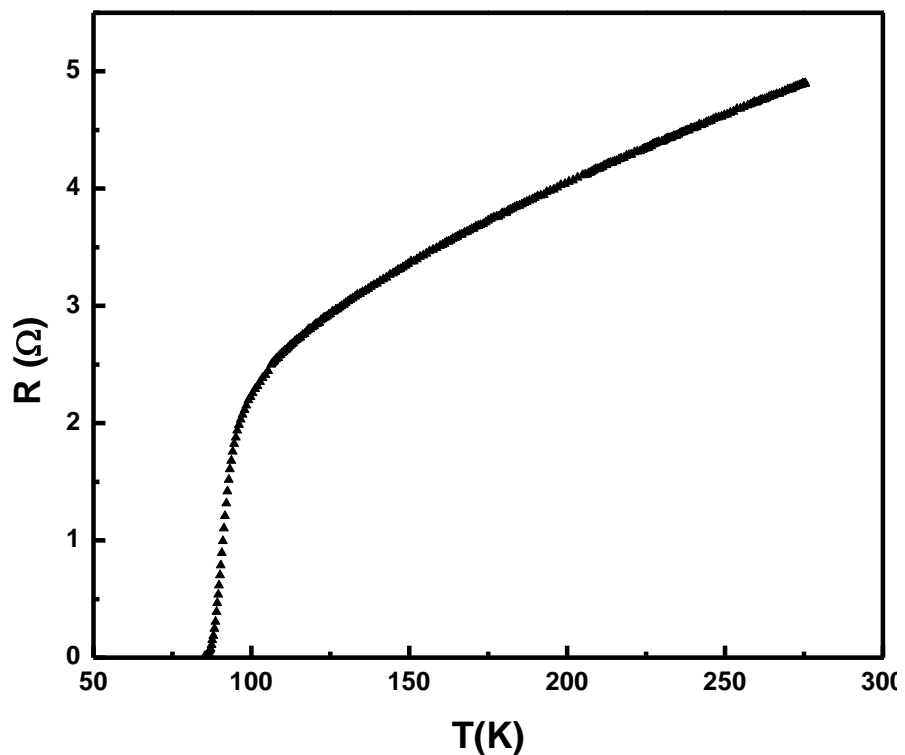


**Figure 4.3:** The resistance as a function of temperature for BSCCO thick tape (sample 46).

The temperature dependences of the electrical resistivity in vortex state with (or without) applying different magnetic fields are plotted as  $R$  versus  $1/T$  in semi log scale as shown in Figure 4.4. The resistance of the vortex state can be written in the form of Arrhenius relation as:

$$R(T) = R_0 \exp\left(\frac{-U_0}{k_B T}\right) \quad (4.5)$$

where  $U_0$  is the activation energy.

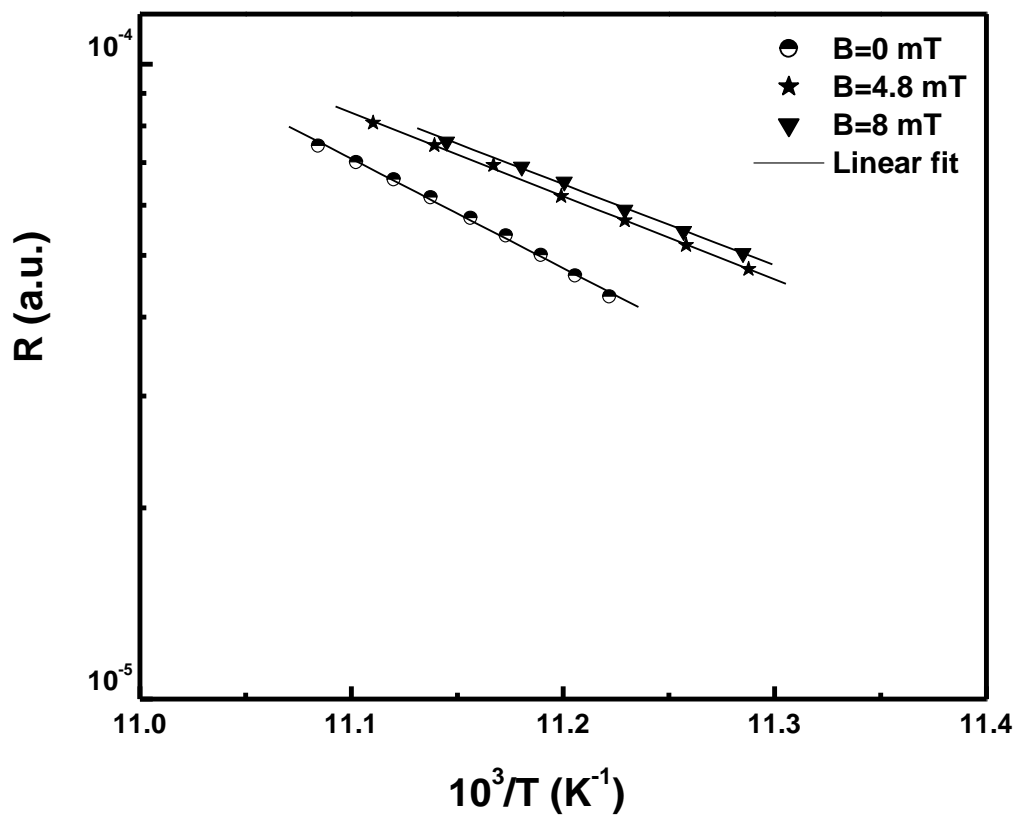


**Figure 4.4:** A semi log dependence of resistance on inverse of temperature ( $1/T$ ) for thick tape sample at different fields.

This relation suggests that the dominant dissipating mechanism is thermally activated flux motion as suggested by Kes *et al.*, (1990). The activation energy  $U_0$  could be determined from the slope of the  $\ln R$  versus  $1/T$  graph. Fitting the data allows us to estimate the activation energy that was found to vary in between 10 and 200 meV, depending on growth conditions and applied field. Pekala *et al.* (1995) found that the calculated activation energy for a Pb-free textured Bi-2223 system varies from 20 and 80 meV. They observed  $U_0$  to depend on both temperature and the magnetic field. In general, it decreases by increasing both magnetic field and temperature.

Table 1 displays some typical values of  $U_0$  for samples of different growth conditions, while in Table 2, a complete list of activation energies at different growth conditions is given in Appendix B. The same behavior was found for single phase  $\text{HgBa}_2\text{Ca}_2\text{Cu}_2\text{O}_{8+\delta}$  superconductor (Liu *et al.*, 2003) and for  $\text{Bi}_2\text{Sr}_2\text{CaCu}_2\text{O}_{8+x}$  thin films (Attanasio *et al.*, 1995). In addition, Pekala *et al.* (1995) observed that the activation energy is 20 - 30 % higher when a magnetic field is applied along the **a**-axis than  $U_0$  when the field is applied parallel to the **c**-axis. This behavior may be attributed to the large anisotropy that characterized the sample.

Sample	Growth conditions	$U_0$ (m eV) ( $B = 0$ mT)	$U_0$ (m eV) ( $B = 4.8$ mT)	$U_0$ (m eV) ( $B = 8$ mT)
46 (bulk)	Quenched	271.38	186.91	155.75
44 (bulk)	Quenched-annealed	296.44	192.10	170.40
13 (laser cut)	Annealed then etched	34.20	30.39	26.30

**Table 4.1:** Typical activation energy values for different BSCCO samples.

The effect of magnetic field on the resistance of the normal and vortex state and on  $T_c$ , was investigated by applying a small magnetic field parallel to the  $c$ -axis (perpendicular to  $ab$ -plane). Figure 4.5a displays the dependence of the resistance of the normal and vortex states on the applied magnetic field. We can see that the resistance of the sample (thick tape sample) does not change by increasing the field in the range between room temperature and the beginning of the transition to the superconducting state. This may be attributed to the full penetration of the magnetic flux lines to the entire specimen in the normal state (Saleh *et al.*, 1997).

In the transition period, the specimen is expected to be in the mixed state (vortex) in which it is composed of both normal and superconducting states. In this region, the resistance of the sample is strongly dependent on the applied magnetic field as could be noticed from the Figure 4.5 b.

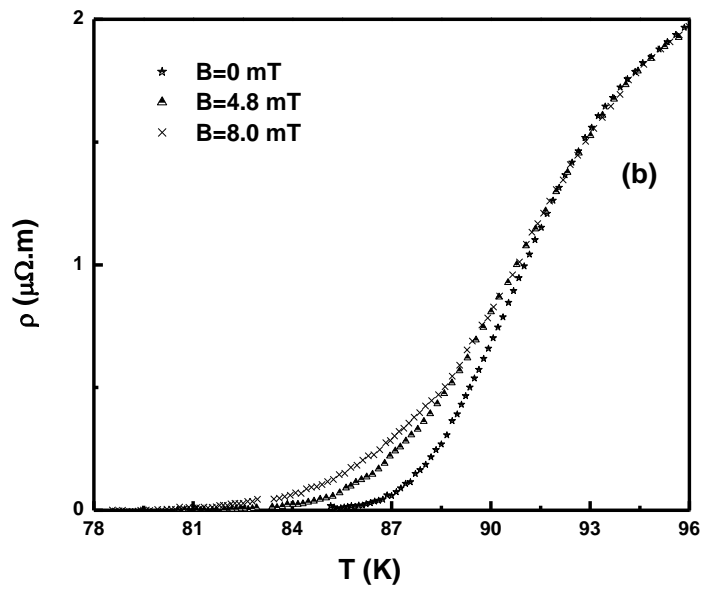
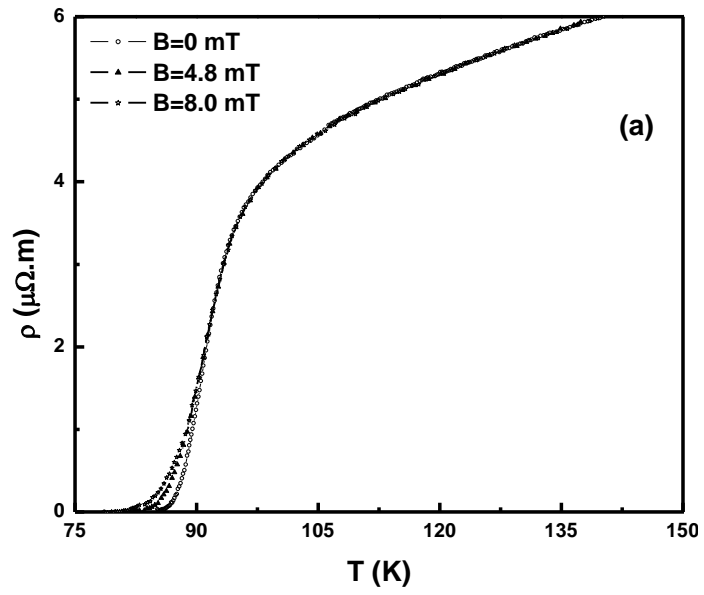


**Figure 4.5:** a) A typical dependence of resistivity of the normal state on the applied magnetic field, and b) Shows the effect of magnetic field on the mixed state for the same sample.

As the field strength is increased, the superconducting state  $T_c$  is lowered and the resistivity curve develops a tail regime slowly varying over a wide temperature range. This broadening behavior is expected for polycrystalline sample due to weak coupling between crystallites (grains) of the sample. Similar results have also been reported for single crystal samples of BSCCO (Plastra *et al.*, 1989), bulk BiPbSCCO sample (Gridin *et al.*, 1990), YBCO and BSCCO thin films (Kobayashi *et al.*, 1989) and in polycrystalline  $Ru_2Gd_2BaCu_2O_8$  (Ru-2212) superconductor (Saleh *et al.*, 2003). Maeda *et al.* (1991) attributed the appearance of finite resistance under the influence of magnetic field mainly to the large fluctuation effect that leads to resistive broadening. In other words, the flux flow resistance will be added to the normal resistance and therefore shifting the critical transition temperature to the left. As the field is increased, more flux lines will be removed thus intensifying the flux flow resistance (Saleh *et al.*, 1997).

More information about the shape of the resistive transition can be obtained by studying the variation of  $dR/dT$  with temperature. The point at which the first derivative of the resistivity curve reaches its maximum value could be selected to define critical temperature  $T_c$ . This point corresponds to the inflection point or the point of rapid change on the original curve (Nkum and Datars, 1992; Poole *et al.*, 1988). The width  $\Delta T$  between the points where the first derivative curve is half of its

maximum value shown in Figure 4.6, is in a good quantitative measure of the width of the transition. The full width at half maximum (FWHM) is equal to 6 K for the present sample (see figure 4.6). The width of the transition is presumably related to the distribution of  $T_c$  among grains (Nkum and Datars, 1992), or in other words to the quality of the sample. That is, the smaller is the width; the better is the quality of the sample. The large sharp peak observed in the curve corresponds to the superconducting transition occurring inside the grains; while the shoulders in the  $dR/dT$  against  $T$  curve are a signature of weak links (boundaries) between grains (Nkum and Datars, 1992). For bulk samples, a secondary peak in the tail was observed. The secondary peak was demolished by the application of magnetic field and the curves thus get broader (Goldschmidt, 1989; Nkum and Datars, 1995; Pekala *et al.*, 1995; Burin *et al.*, 1996). The appearance of the secondary peak was attributed to the deficiency of oxygen molecules in grain boundaries and it was reduced or even eliminated by annealing the sample in oxygen atmosphere (Goldschmidt, 1989).

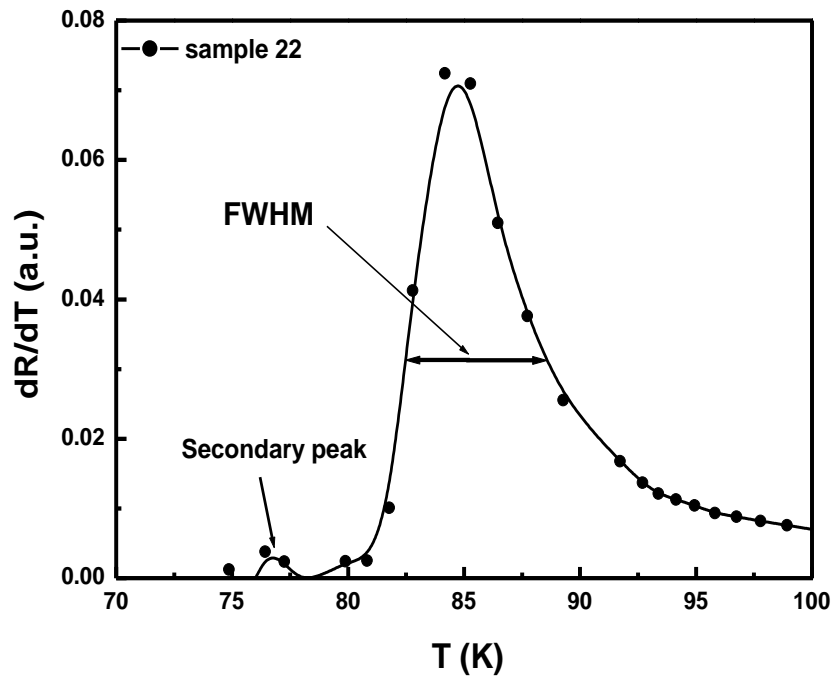


**Figure 4.6:** The resistance first derivative dependence on temperature.

The second derivative showed in Figure 4.7 permits the precise measurement of the transition temperature. The transition temperature occurs when the curve crosses the base line. In addition, the curve of the second derivative gives the peak-to-peak width,  $\Delta T_{pp}$  of the distribution of grains (Poole *et al*, 1988). For our sample the peak-to-peak transition width,  $\Delta T_{pp}$  is 4.1 K. This result is in good agreement with the results obtained for a Ge-doped Bi-Pb-Sr-Ca-Cu-O system, with transition width  $\Delta T_{pp}$  ranges from 4 - 6.7 K (Nkum and Datars, 1992). Nkum and Datars (1995) also found that the transition width  $\Delta T_{pp}$  for In-doped Bi- Pb-Sr-Ca-Cu-O system ranges between 4.3 - 5.2 K depending on In concentration.

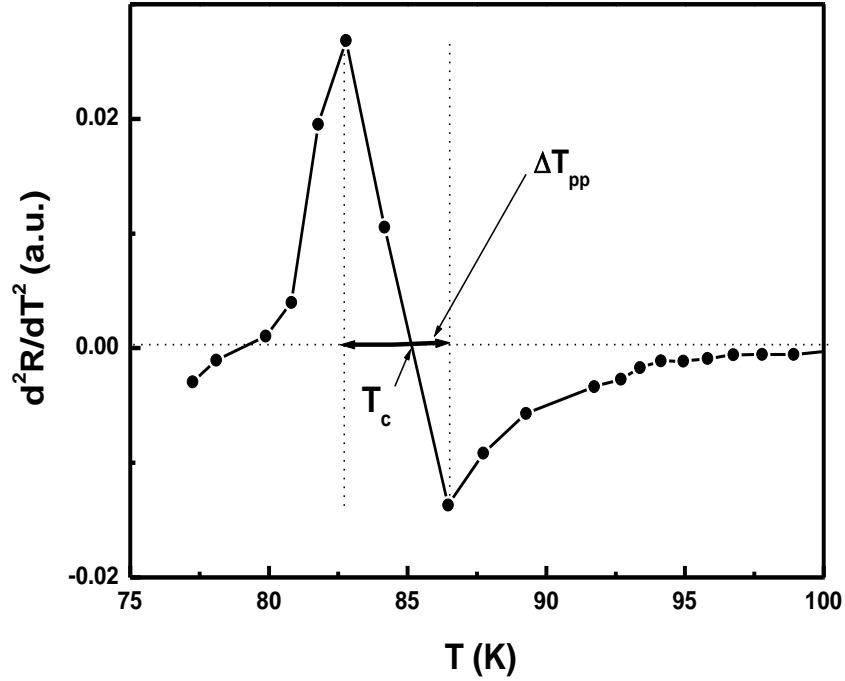


**Figure 4.7:** Temperature dependence of the resistance second derivative for BSCCO thick tape sample.

The critical current  $I_c$  is found to be affected greatly by temperature, magnetic field and growth conditions. The critical current as a function of temperatures is plotted in Figure 4.8 for a laser cut sample (sample 22). The sample showed a slow increase of  $I_c$  for temperatures close to  $T_c$ , however a larger increase is observed below  $\sim 50$  K.

In addition, the figure shows a theoretical fit of data according to a relation of the form:

$$I_c(T) = I_0 \left( 1 - \frac{T}{T_c} \right)^n \quad (4.6)$$

where  $I_0 = 20$  mA. The fitting parameters are  $n = 1.76$  and  $T_c = 82$  K. The value of  $n$  indicates that the intergrain junctions of our sample behave as SNS (superconductor-normal-superconductor) ones. Similar results were obtained for a Pb doped Bi-2223 ceramic but with  $n = 1.9$  (Gonzalez *et al.*, 1995).

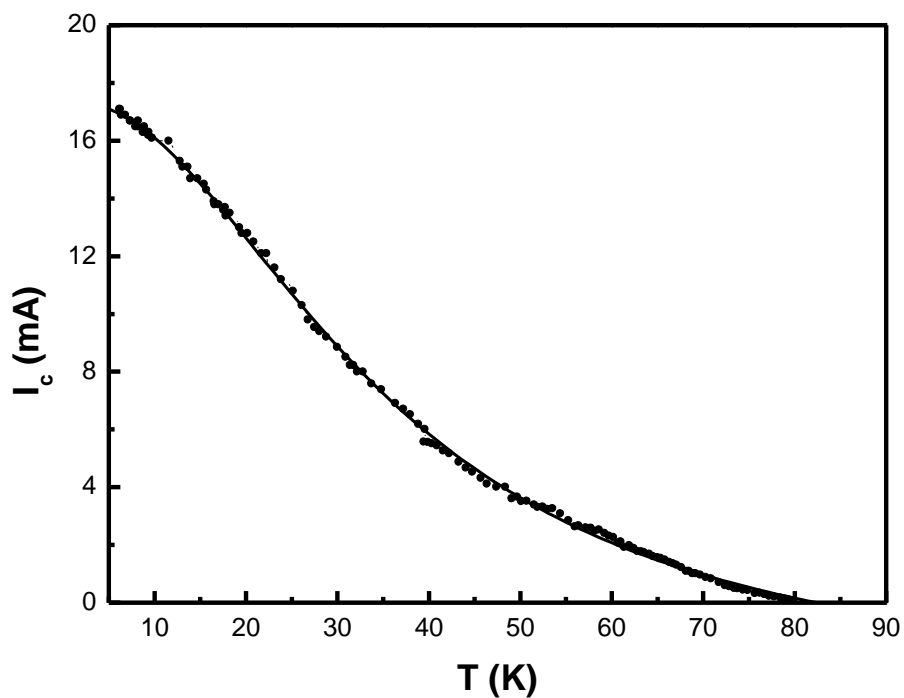


**Figure 4.8:** Temperature dependence of the transport critical current for Bi-2212 laser cut sample.

The growth conditions and the applied magnetic field were found to affect greatly the critical current density. Figure 4.9a displays the  $J_c$  versus the magnetic field for two different samples grown under different growth conditions at fixed temperature. A quenched sample (sample 46) and a quenched then annealed sample (sample 44). The  $J_c$  data for sample 46 was taken at 78 K, while for sample 44 at 75 K. As shown in

the figure,  $J_c$  decreases slowly with increasing the magnetic field strength near  $T_c$ . The same behavior of  $J_c(B)$  was found for  $(\text{Bi,Pb})_2\text{Sr}_2\text{Ca}_2\text{Cu}_3\text{O}_x$  silver-sheated tapes (Hensel *et al.*, 1993),  $\text{Bi}_{2.2}\text{Sr}_{1.8}\text{Ca}_2\text{O}_{8.2}$  single crystal (Hayashi *et al.*, 1990), and in bulk  $\text{Bi}_{1.6}\text{Pb}_{0.4}\text{Sr}_2\text{Ca}_2\text{Cu}_3\text{O}_{10}$  (Umemura *et al.*, 1990). Umemura and coworkers (1990) attributed the abrupt degradation in  $J_c$  with increasing temperature and magnetic field to the influence of the significant flux creep due to a large thermal energy and weak pinning energy.

The data of Figure 4.9a is replotted on a semi-log graph as displayed in Figure 4.9b. A good linear fit for  $\log J_c$  with the applied magnetic field is obtained. It can be easily seen from the Figure that  $J_c(B)$  exhibits an approximate dependence on  $B$  as:

$$J_c(B) = J_{c_0} \exp\left(-\frac{B}{B_0}\right) \quad (4.7)$$

where  $J_{c_0}$  is the critical current density at zero field and  $B_0$  is a constant field that prevents the divergence of  $J_c$  at  $B = 0$  T. The same relation was observed for a Bi-2223 tape for field perpendicular to  $c$ -axis ( $B \perp c$ ), and for field parallel to  $c$ -axis ( $B \parallel c$ ) (Kung *et al.*, 1995). Such an exponential decay of  $J_c$  with  $B$  is an evident of the strong flux pinning centers in the sample.

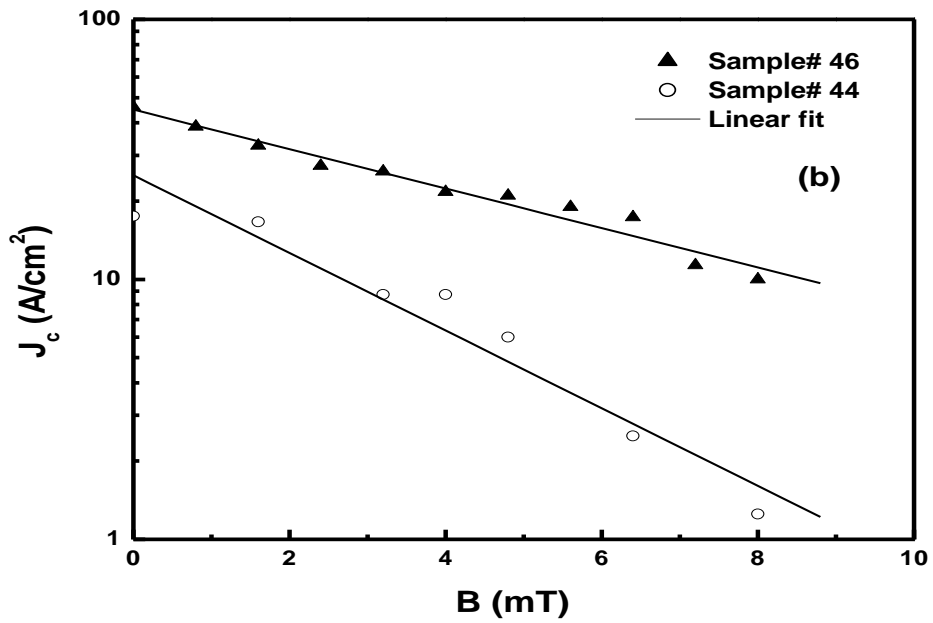
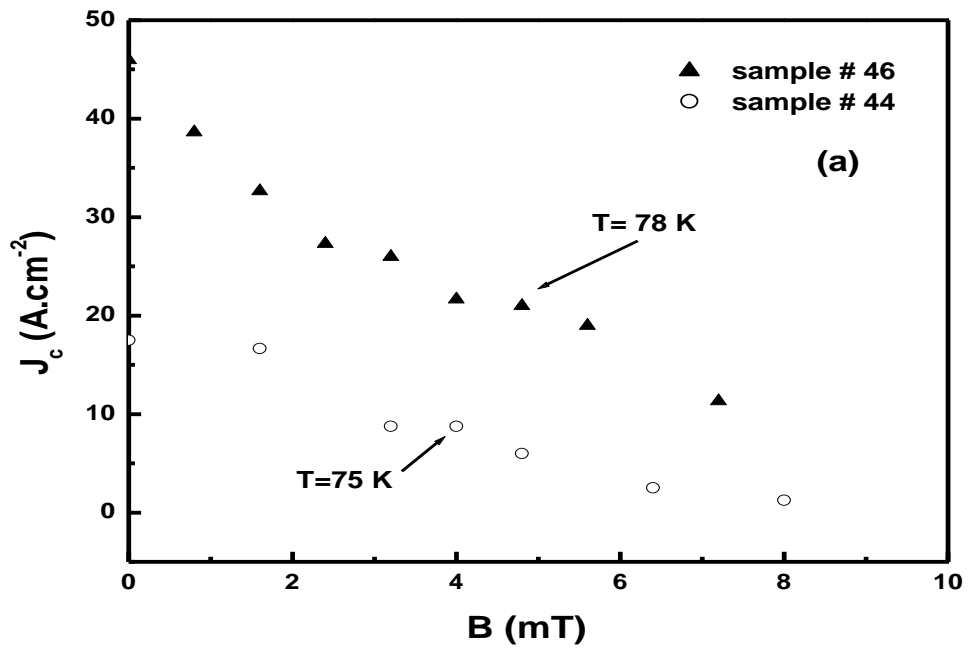


**Figure 4.9:** a) The critical current density versus magnetic field for two different Bi-2212 bulk samples.

b) A semi log plot of  $J_c$  versus the applied magnetic field for the same two samples in (a) with a linear fit.

The influence of growth conditions such as heat treatment conditions, substrate type, annealing and grain size on electrical and magnetic properties were also investigated for Bi-2212 thick tapes. Figure 4.10 represents the temperature dependence of critical current densities of two samples grown under different heat treatments. As can be seen from the figure, the critical current density of quenched and annealed sample for several hours at 500 °C is higher than that obtained for only quenched superconducting sample. Annealing in N<sub>2</sub> atmosphere can improve coupling between grains, hence increasing J<sub>c</sub>. Noji *et al.* (1993) observed that annealing in N<sub>2</sub> at (500 - 600 °C) could improve the T<sub>c</sub> value of the superconductor by reducing the excess of oxygen content, therefore improving the intergranular coupling properties of the samples. Moreover, J<sub>c</sub> was found to strongly decrease with annealing time periods (Dimesso *et al.*, 1992). In addition, quenching the specimen from 840 °C to room temperature may increase the electrical parameters of the superconductor. It resulted in a higher transition temperature, and in higher critical current density, J<sub>c</sub> (Saleh *et al.*, 1997).

The type of substrate material was found to be very important and critical in the formation of the superconducting phase. There are several good substrate environments for the formation of Bi-2212 superconducting phase such as: silver foil, single crystal MgO and single crystal MgO coated with thin silver layer (Saleh *et al.*, 1997). Also Ag-

Au alloys are a good and superior substrate materials of Bi-2212 for power current (super current) leads in superconducting magnets (Nomura *et al.*, 1993). Furthermore, Fujishiro *et al.* (1993) reported that the addition of Au was very effective in decreasing the thermal conductivity of the superconductor.

The amount of silver added to the sample has a strong influence on the  $J_c$ . Figure 4.10 shows the influence of Ag on critical current density for samples grown on MgO substrate covered with 1  $\mu\text{m}$ -silver (a) and 0.5  $\mu\text{m}$ -silver (b). As it could be seen from the figure,  $J_c$  for the sample grown on MgO coated with 1  $\mu\text{m}$  silver layer is much greater than  $J_c$  for the sample grown on MgO coated with 0.5  $\mu\text{m}$  silver layer. This behavior may be attributed to dependence of the melting point of Bi-2212 oxide on the substrate material (Togano *et al.*, 1991). It was reported that silver substrate plays an important role in the grain alignment, by lowering the melting point of the oxide and in the formation of highly textured microstructure (Kase *et al.*, 1991; Togano *et al.*; 1991; Zhang and Hellstorm, 1993). Zhang and Hellstorm, (1993) found that the thickness of the tape was very important in aligning the grains and in increasing  $J_c$ , they observed a highly aligned texture for tapes of thickness less than 25  $\mu\text{m}$ , while it was less pronounced for tapes of thickness

greater than 25  $\mu\text{m}$ . This suggests that thinner films have fewer and smaller second phases and better alignment of the grains.

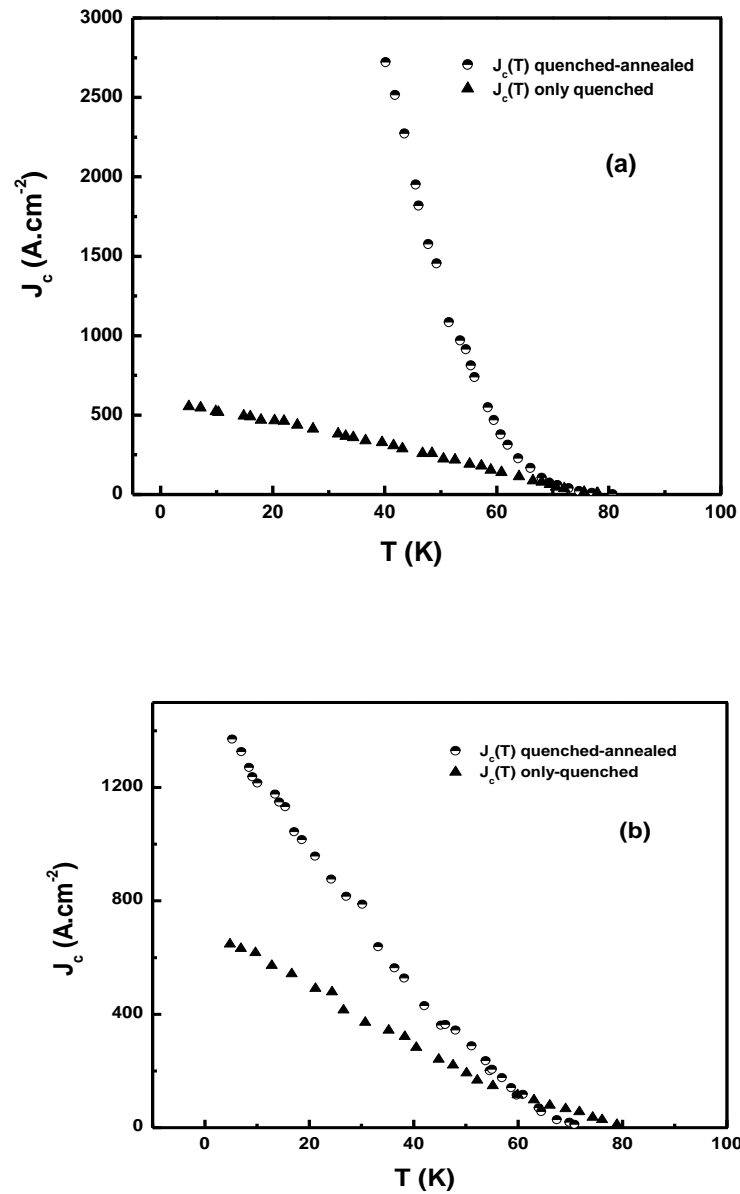


**Figure 4.10:** The effect of heat treatment conditions and silver addition on the critical current density of Bi-2212 thick tapes. a) The samples grown on MgO substrate covered by  $1\ \mu\text{m}$  silver layer, and b) The samples grown on MgO substrate covered by  $0.5\ \mu\text{m}$  silver layer.

The grain size also has a large influence on the determination of  $T_c$  of the superconducting state and the resistivity of the normal state. Larger grains will have lower resistivity in normal state and higher critical  $T_c$  than those of smaller grain size (Saleh *et al.*, 1997). In addition, grain size and grain boundaries will be greatly affect the critical current dependence on both temperature and magnetic field (Saleh *et al.*, 1998<sup>b</sup>)

The study of IVCs is very important in determining the  $J_c$  and other electrical behavior of the sample. Typical IVCs of Bi-2212 phase in a zero applied magnetic field is displayed in Figure 4.11.

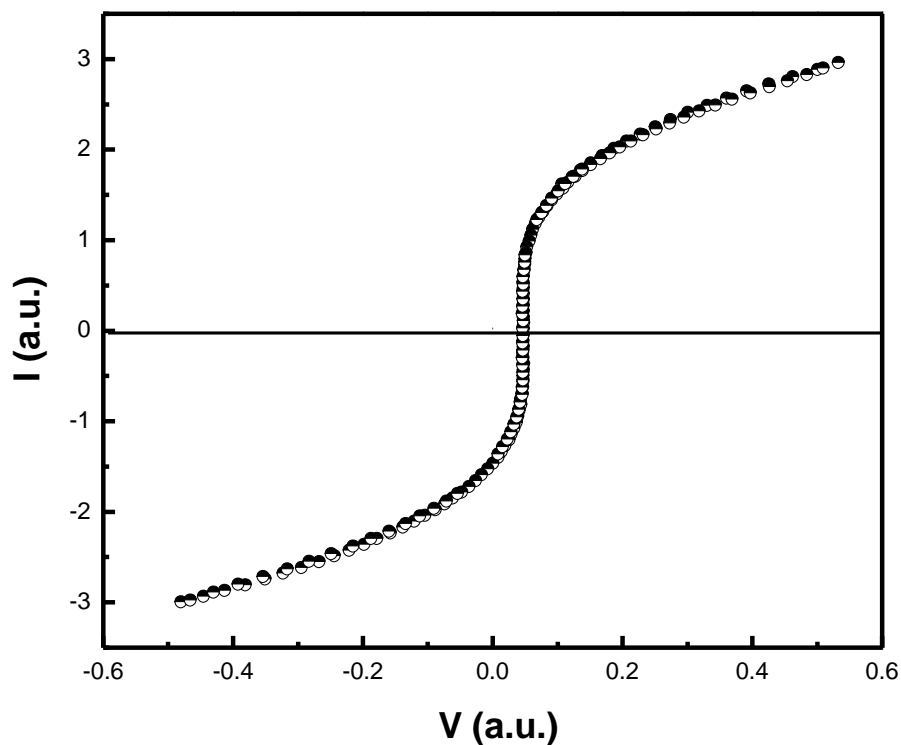


**Figure 4.11:** A typical IVCs of Bi-2212 superconductor thick tape.

The figure shows that nonlinearity of I-V curve is observed for I very close to  $I_c$  and become linear above the critical current  $I > I_c$ . Flux creep is assumed to be the main source of nonlinearity of  $V(I)$  at small V in BSCCO (Warnes *et al.*, 1986). The same behavior of IVCs was also observed in a single grain or polycrystalline bridges (Zitkovsky *et al.*, 1991). The critical current  $I_c$  can be determined from this curve by taking the average value at both ends of the curve when the voltage starts to develop a cross the sample (Saleh *et al.*, 1997).

The IVCs were measured for several samples grown under different growth conditions. The linear portion ( $I > I_c$ ) of the voltage is taken; the data is then replotted on a log-log plot, and then fitted to a certain scale law. It is found that the voltage dependence of the current is well expressed by a relation of the form:

$$\mathbf{I} \sim \mathbf{V}^{\beta} \quad (4.8)$$

where  $\beta$  is an exponent, determined from the slopes of the I-V curve shown in Figure 4.12. In general, its value was found to be in the range from 0.1 - 0.5 (as was found by fitting the data in Figure 4.12a and b). Figure 4.12a shows the IVCs in log-log scale for same sample at zero magnetic fields and at different temperatures 80, 77 and 76. In Figure 4.12b, the IVCs for different samples grown under different growth conditions. The figure also shows a clear power law behavior in the

mean-field transition temperature region. Same results were found for (Bi-Pb)-Sr-Ca-Cu-O single crystal (Pradhan *et al.*, 1993).

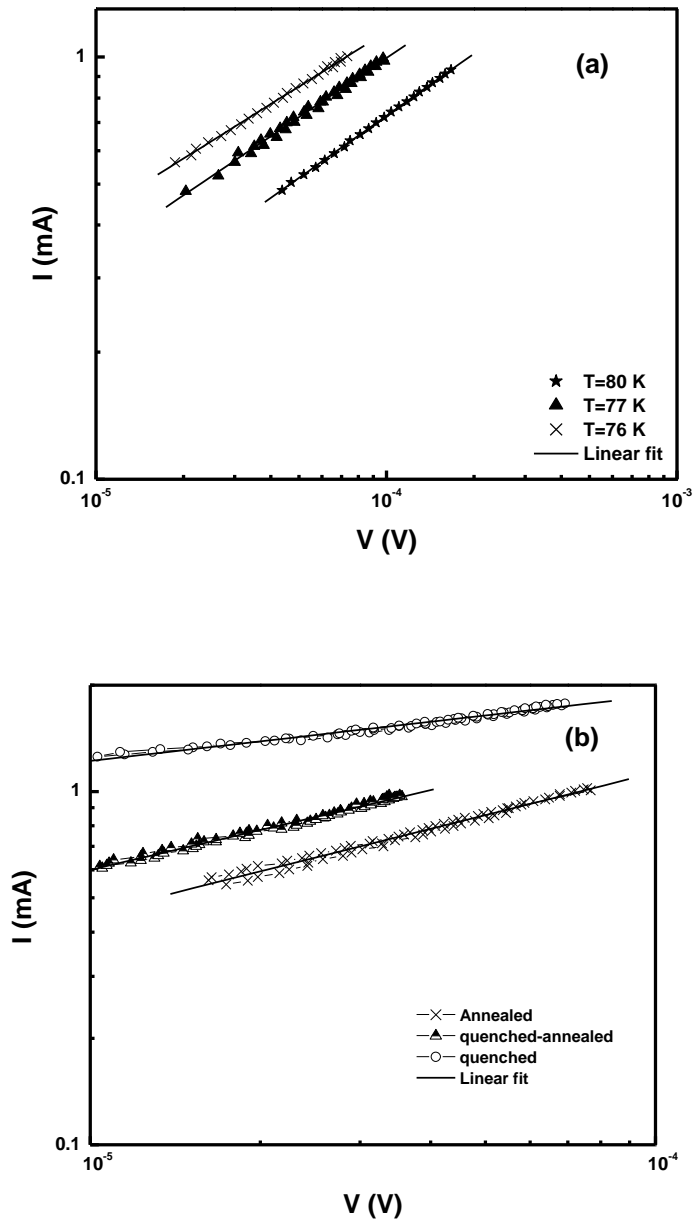


**Figure 4.12:** I-V characteristics in log-log scale for: a) same sample at zero magnetic fields at different temperatures and b) for different samples grown under different growth conditions.

The IVCs are influenced greatly by the applied magnetic field. Figure 4.13 shows the IVCs on a log-log scale of Bi-2212 thick tape (quenched-annealed sample (sample 44)) in various magnetic fields at different temperatures. By fitting the data, the slope of lines is found to be in the range 0.94 - 1.

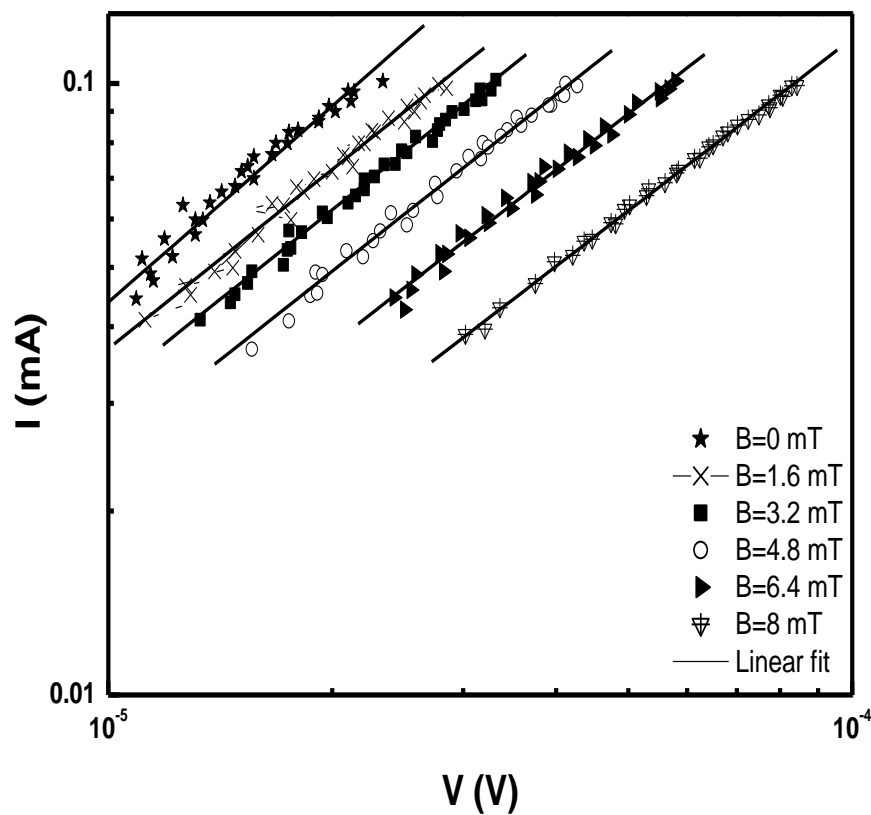


**Figure 4.13:** IVCs in log-log scale of quenched-annealed Bi-2212 thick tape sample at various magnetic fields and temperatures.

In order to study the dependence of the magnetic field on IVCs and more precisely, we made a log-log plot of the current versus the applied

magnetic field at different fixed voltages (0.35 mV, 0.3 mV, 0.25 mV and 0.185 mV). The results were shown in Figure 4.14. The current  $I(B)$  at constant voltage decreases with the application of the magnetic field according to the relation:

$$I(B) \sim e^{-cB/B^*} \quad (4.9)$$

Qualitatively, our results are consistent with the results observed for (Bi-Pb)-Sr-Ca-Cu-O single crystal (Pradhan *et al.*, 1993), Bi-2223 silver sheathed tape, and for Bi-2212 silver sheathed tape with (Gurevich *et al.*, 1993).

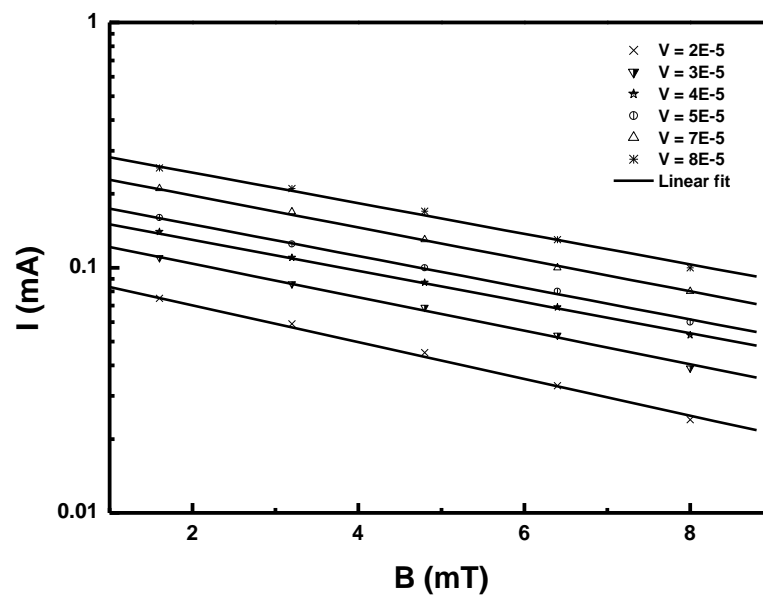


**Figure 4.14:** Dependence of current on applied magnetic field in log-log scale at different fixed voltages, for Bi-2212 thick tape.

Heat treatment conditions affect greatly the IVCs behavior. Figure 4.15 displays the IVCs on log-log scale for two different heat treatment

samples; sample 46, a quenched sample (Figure 4.15 a) and sample 44, a quenched then annealed sample (Figure 4.15 b). Two qualitatively different I-V curves can be observed in this figure at low applied fields, 0 mT, 1.6 mT, and 4.8 mT, respectively. Sample 44 shows a power law dependence whose slope is equal to 1, while sample 46 shows a two distinct power laws. At low fields and low voltage, a power law with slope equal to 0.3 is observed, whereas at higher voltages and low fields a power law with slope equals to 0.42 is observed. This change of slope may be attributed to the different distribution of vortices states within the sample (Sun *et al.*, 1991).

The relation between current and voltage could be written in the form:

$$I \propto \begin{cases} V^{\beta_1}, & \text{with } \beta_1 \approx 1, \text{ for sample 44 at fields } 0, 1.6, 4.8 \text{ mT} \\ V^{\beta_2}, & \text{with } \beta_2 \approx 2, \text{ for sample 46 at fields } 0 \text{ and } 1.6 \text{ mT} \\ V^{\beta_3}, & \text{with } \beta_3 \approx 3, \text{ for sample 46 at fields } \geq 4.8 \text{ mT} \end{cases}$$

(4.10)

It was also found that a relation related the current to the magnetic field:

$$I(\mathbf{B}) \sim e^{-c\mathbf{B}/B^*} \quad (4.11)$$

So the general current dependence on field and voltage could be written in the form:

$$I \sim v^\beta e^{-c\mathbf{B}/B^*} \quad (4.12)$$

or 
$$I = m v^\beta e^{-c\mathbf{B}/B^*} \quad (4.13)$$

Therefore, the current is directly proportional to the voltage and inversely proportional to applied field.

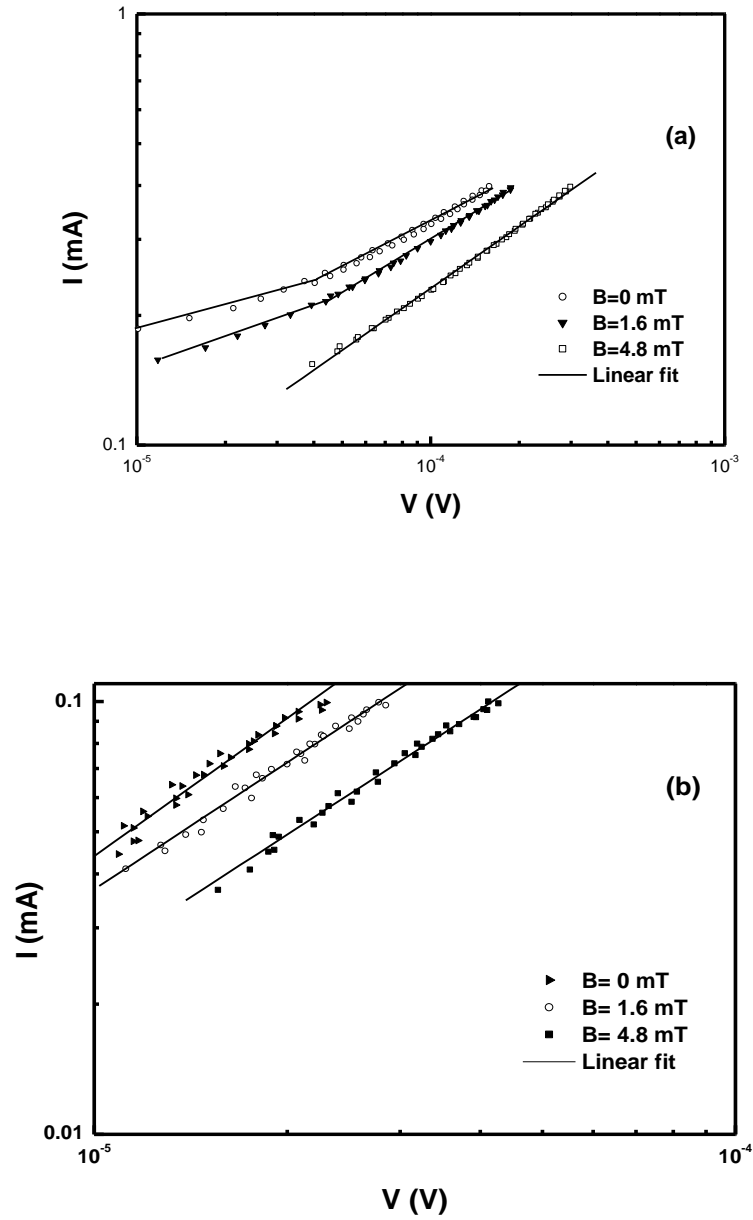


**Figure 4.15:** I-V characteristics for two different samples, grown under different heat treatment conditions (a) quenched-annealed sample (b) only quenched sample.

## Chapter Five

### Summary and Future Work

A study of the vortex state of the high- $T_c$  superconductor  $\text{Bi}_2\text{Sr}_2\text{CaCu}_2\text{O}_x$  thick tapes was carried out. The temperature dependence of the electrical resistivity, the IVCs and  $I_c$  were investigated for several samples with different heat treatment conditions and with or without applied magnetic fields. The resistance was found to behave as an Arrhenius-like relation,  $R = R_0 \exp(-U_0/kT)$  with activation energy  $U_0$  in the range 10 - 200 meV. The activation energy values were strongly dependent on growth condition, heat treatment conditions and the applied magnetic field.

The current dependence on voltage can be expressed by a power law relation of the form  $I \sim V^\beta$  with exponent  $\beta$  in the range of 0.5 - 1, depending on growth conditions of the sample. The current at constant voltages was also found to decay exponentially with increasing the magnetic field. Heat treatment conditions also affect greatly the IVCs behavior in the presence of magnetic fields. Two qualitatively different I-V curves were observed for two different heat-treated samples. This type of behavior was attributed to the different distribution of vortex states within the sample.

$J_c$  was found to be affected by heat treatment conditions also. Higher  $J_c$  values were observed for quenched, then annealed samples than those for only quenched samples. In addition, annealing in  $N_2$  has increased  $J_c$  values, while the amount of silver added to the sample has also a strong influence on  $J_c$ . The type of substrate material was found to be very important and critical in the formation of the superconducting phase.

The work presented in this thesis can be extended to include the effect of different fields and growth conditions on the IVCs for other different systems such as YBCO, HgBCCO, Pr (Nd) BCO and RSGCO. In addition, more precise measurements should be carried out to examine the vortex distribution within the flux lattice.

## References

Attanasio C., Coccrese C., Kushnir V., Maritato L., and Prischepa S., *Physica C* **255** (1995) 239.

Balestrino G., **Superconductivity**, editors, S. Space and M. Acquarone (1989) 495.

Bock J., Elschner S., and Preisler E., **Advances in superconductivity III**, (1990) 797.

Burin J., Dehmej J., Fouad Y., Raboutou A., Peyral P., Lebeau C., Rosenblatt J., Carel C., and Oummou A., *Solid state communications*, **99** (1996) 531.

Chakrabarti M., Sarkar A., Chattapadhyay S., Sanyal D., Prahan A., Bhattacharya K., and Banerjee D., *Solid state communications*, **128** (2003) 321.

Dimesso L., Masini R., Cavinato M., Fiorani D., Testa A., and Auriscchio C., *Physica C* **203** (1992) 403.

Doss J., **Engineer's guide to high-temperature superconductivity**, (1989), John Wiley & Sons, New York, USA.

Flippen R., Askew T., and Osofsky M., *Physica C* **201** (1992) 391.

Fujishiro H., Ikebe M., Noto K., Sasoka T., and Nomura K., *Cryogenics* **33** (1993) 1086.

Goldschmidt D., *Phys. Rev. B* **39** (1989) 2372.

Genes P., *Rev. Mod. Phys.* **36** (1964) 225.

Gibson K., Ziegler P., and Meyer H., *Supercond. Sci. Technol.* **17** (2004) 786.

Gonzalez J., Mune P., Flores L., and Altshler E., *Physica C* **255** (1995) 6.

Grader G., Georgy E., Gallagher P., O'Bryan H., Johnson D., Sunshine S., Zahurak S., Jin S., and Sherwood R., *Phys. Rev. B* **38** (1988) 757.

Gridin V., Krause T., and Datars W., *J. Physics: Condensed Matter* **2** (1990) 8755.

Gurevich A., Pashitski A., Edelman H., and Larbalestier D., *Appl. Phys. Lett.* **62** (1993) 1688.

Han G., Ong C., and Li H., *Physica C* **211** (1993) 279.

Hayashi S., Shibusaki K., Shigaki I., Fukumoto Y., Kjikawa H., Ogawa R., Kawate Y., Maret V., Kitahama K., and Kawai S., **Advances in superconductivity III**, (1990) 495.

Hensel B., Grivel C., Jeremie A., Perin A., Pollini A., and Flukiger K., *Physica C* **205** (1993) 329.

Holesinger T., Miller D., and Chumbley L., *Physica C* **217** (1993) 85.

Ishizuka Y., Terashima Y., and Miura T., **Advances in superconductivity III**, (1990) 1065.

Jin H., Hu Z., Ge Y., Liu Q., Liu C., and Shi C., *Physica C* **211** (1993) 49.

Kase J., Morimoto T., Togano K., Kumakura H., Dietderich D., Maeda H., *IEEE Trans. Magn.* **27** (1991) 1254.

Kes P., Aarts J., Vinokur V., and Vander Beek C., *Phys. Rev. Lett.* **64** (1990) 1063.

Khan D., *Physica C* **222** (1994) 233.

Kittel C., **Introduction to solid state physics**, 7<sup>th</sup> edition, (1996), John Wiley, New York, USA.

Kleiner R., and Muller P., *Phys. Rev. B* **49** (1994) 1327.

Kobayashi N., Iwasaki H., Kawabi H., Watanabe K., Yamane H., Kurosawa H., Masumoto H., Hirai H., and Muto Y., *Physica C* **159** (1989) 295.

Kobel S., Schneider D., Sager D., Sutterlin P., Fall L., and Ganckler L., *Physica C* **399** (2003) 107.

Kumakura H., Togano K., Maeda H., Kase J., and Morimoto T., *Appl. Phys. Lett.* **58** (1991) 2830.

Kung P., Mchenry M., Maley M., Kes P., Laughlin D., and Mullins W., *Physica C* **249** (1995) 53.

Lee H., Kim C., Lee K., and Won D., *Appl. Phys. Lett.* **54** (1989) 391.

Lee H., Hosono H, Nakamura K and Abe Y, Physica C **185-189** (1991) 2389.

Liu S., Wu G., Xu X., Wu J., and Shao H., Solid State Communications **127** (2003) 749.

Maeda A., Watanabe H., Tuskada I., Terasaki I., Uchinokura K., Obara H., and Kosaka S., Supercond. Sci. Technol. **4** (1991) S337.

Maeda A., Noda K., Uchinokura K, and Tanaka S., Japanese Journal of Applied Physics, **28** (1989) L576.

Maeda H., Tanaka Y., Fukutomi M., and Asano T., Jpn. J. Appl. Phys. **27** (1988) L209.

Martin S., Fiory A., Fleming R., Espinosa G., and Cooper A., Phys. Rev. Lett. **62** (1989) 677.

Moehlecke S., Westphal C., Torikachvili M., Davis J., and Torriani I., Physica C **211** (1993) 113.

Mulary L. N., **Magnetic susceptibility**, (1963), John Wiley and Sons, USA.

Müller K., Ricketts B., Macfarlane J., and Driver R., Physica C **162-164** (1989) 1177.

Natividad E., Angurel L., Anders J., and Mayoral M., Supercond. Sci. Technol. **17** (2004) 308.

Nkum R., and Datars W., Physica C **190** (1992) 465.

Nkum R., and Datars W., Supercond. Sci. Technol. **8** (1995) 822.

Noji H., Zhou W., Glowacki B., and Oota A., Physica C **205** (1993) 397.

Nomura K., Seido M., Kitaguchi H., Kumakura H., Togano K., and Maeda H., Appl. Phys. Lett **62** (1993) 2131.

Pekala M., Bougrine H., Lada T., Marawski A., and Ausloos M., Supercond.Sci. Technol. **8** (1995) 726.

Pena O., Dinia A., Perrin C., Perrin A., and Sergent M., Physica C. **162-164** (1989) 1215.

Plastra T., Batlogg B., Vandover R., Schneemeyer L., and Waszczak J., Appl. Phys. Lett. **54** (1989) 763.

Poole P., Datta T., and Frach A., **Copper-oxide superconductors**, (1988). John Wiley and Sons, New York, USA.

Prabhu P. S., Rao M. S., and Rao G. V., Physica C **211** (1993) 279.

Pradhan A., Hazell S., Hodby J., Chen C., Hu Y., and Wanklyn B., Physica C **204** (1993) 325.

Pureur P., Schaf J., Gusamao M., and Kunzler J., Physica C **176** (1991) 357.

Ray A., Dey T., and Ghatak S., Journal of Superconductivity, **15** (2002) 201.

Rose I., and Rhoderick E.H, **Introduction to superconductivity**, (1994), BpC Wbeatons Great Britain.

Saleh A. M, Schindler G., Sarma C., Kingon A., and Haase D., Bethlehem Univercity Journal **16** (1997) 46.

Saleh A. M, Schindler G., Sarma C., Haase D., Koch C., and Kingon A., Physica C **295** (1998)<sup>a</sup> 225.

Saleh A. M, Abhath Al-Yarmouk, Pure.SCi. & Eng. **7** (1998)<sup>b</sup> 37.

Saleh A. M., Abu-Samreh M. M., Leghrouz A. A., Physica C **384** (2003) 383.

Shimoyama J., Kase J., Morimoto T., Kitaguchi H., Kumakura H., Togano K., and Maeda H., Japn. J. Appl. Phys **31** (1992) L1167.

Sun J., Eom C., Larison B., Bravman J., and Geballe T., Phys. Rev. B **43** (1991) 3002.

Tinkham M., **Introduction to superconductivity**, 2<sup>nd</sup> edition, (1996), McGraw-Hill, New York, USA.

Tinkham M., and Lobb C., Solid state physics. **42** (1989) 91.

Togano K., Kumakura H., Dietderich D., Maeda H., Kase J., and Nomura K., Sendai, Japan, Springer-Velag (1991) 619.

Umemura T., Egawa K., Wakata M., Utsunomiya S., Ni B., Takeo M., Yamafuji K., Otabe E., and Matsushita T., **Advances in superconductivity III**, (1990) 507.

Varma K., Rao K., and Rao C., Appl. Phys. Lett. **54** (1989) 69.

Warnes W., and Larbalestier D., Appl. Phys. Lett. **48** (1986) 1403.

Wider W., Bauernfeind L., Braun H, Burkhatdt H., and Rainer D,  
Phys. Rev. **B55**, (1997) 1254.

Xu G., Sun Y., Du J., Zhou Y., Zeng R., Fu X., and Hua P., J. Appl.  
Phys. **18** (1997) 1331.

Yang Y., Beuze C., and Yi Zand Scurlock R., Physica C **201**  
(1992) 325.

Zhang W., and Hellstorm E., Physica C **218** (1993) 141.

Zitkovsky I., Hu Q., Prlando T., Melngailis J., and Tao T., Appl.  
phys. Lett. **59** (1991) 727.

## Appendix A

**Table 1:** Typical A (intercept) and B (slope) values for different samples grown under different growth conditions.

Sample	Growth conditions	A	B
<b>BSCCO thick tape</b>			
QUN-ANL3	Quenched annealed	9.4E-5	2.3E-6
ANL-SILV	Annealed Ag/MgO substrate	3.9E-5	3.9E-7
13 (laser cut)	Annealed then etched	1.8E-4	1E-6
23 (laser cut)	Annealed on MgO substrate only	2.4E-5	1.4E-6
25 (laser cut)	Annealed on Ag/MgO substrate	5.2E-5	1.6E-6

## Appendix B

**Table 2:** Typical values of activation energy ( $U_0$ ) for different samples at different growth conditions, (At zero applied fields).

Sample	Growth conditions	Activation energy $U_0$ (meV)
BSCCO thick tape		
Anl-mg	Annealed sample MgO substrate	443.4
Amgmgol	Annealed sample Ag/MgO substrate	24.0
Anl-Silv	Annealed sample Ag substrate	121.6
21	Annealed then etched (on MgO substrate)	41.6
14	Annealed then etched	18.1
19	Annealed then etched	159.6
13	Annealed then etched	36.0
23	Annealed then etched (on MgO substrate)	68.3
24	Annealed then etched (on MgO/Ag substrate)	30.3

25	Annealed then etched (on MgO/Ag substrate)	32.4
3	Laser cut sample Annealed then etched	14.8
Qun-anl3	Quenched-annealed	21.9
Qun-anl2	Quenched-annealed	163.2
Qun-anl	Quenched-annealed	132.6
Q-analag1	Quenched-annealed	290.7
9	Annealed then etched	10.9
Mg silver	Annealed in N <sub>2</sub>	32.0
4	Annealed at 600 °C	31.8

## Appendix C

Schematic diagrams of the structure of the three phases belonging to the BSCCO family.

